Rev.Adv.Mater.Sci. 19(2009) 13-40

# DISLOCATION MECHANICS ASPECTS OF ENERGETIC MATERIAL COMPOSITES

**R.W. Armstrong**

Center for Energetic Concepts Development, Department of Mechanical Engineering, University of Maryland, College Park, MD 20742, U.S.A.

*Received: November 19, 2008*

**Abstract.** The dislocation mechanics based properties of solid energetic materials, particularly, of high explosives, are of particular interest in connection with issues of intrinsic chemical stability and with their fast chemical decomposition when employed as propellants or in explosive formulations. The ballistic impact and shock-associated plasticity responses of such materials present great experimental and model challenges for establishment of predictable performances. As demonstrated in the present report, much has been learned through direct investigation with a full range of scientific tools of the individual crystal and composite material properties and, also, through their comparison with relevant inert ionic and metallic material behaviors. Thus, in relation to other solid material structures, energetic crystals are elastically compliant, plastically strong, and prone to cleavage fracture. Somewhat surprisingly perhaps for such materials, individual dislocation self-energies are indicated to be relatively large while the intrinsic crystal-determined dislocation mobility is restricted because of the complicated and rather dense molecular packing of awkwardly-shaped molecules that are self-organized within lower-symmetry crystal structures. Because crack surface energies are low, cleavage is able to be initiated by relatively small dislocation pile-ups and, with the restricted dislocation mobility, there is little additional plastic work requirement associated with cleavage crack propagation. Nevertheless, when compared with indentation fracture mechanics prediction, crack propagation appears to be controlled by the behavior of very limited dislocation activity at the crack tip. Adiabatic heating associated with dislocation pile-up avalanches provides an important mechanism for the thermal “hot spot” model of explaining the initiation of rapid chemical decompositions and relates directly to predicted influence of crystal (or particle) sizes. On such basis, desired characteristics of greater mechanical insensitivity to initiation but afterwards greater power dissipation are predicted to occur for energetic composite formulations made from smaller particle-sized ingredients.

## 1. INTRODUCTION

Solid energetic composite materials are included within the category of advanced materials, first, because complete information remains to be determined both for the individual component behaviors and for their interactions in relatively complex formulations; and, secondly, because there is the need for understanding of the composite performances, for example, under mechanics-based high rate loading conditions involving very substantial rates of energy decompositions occurring within a shock wave associated environment. Beginning from the late 19$^{th}$ century until the present time, much chemical- and physics-based information has been gained on the component and formulated energetic material properties and uses. More recently, additional information has been gained through a material science approach of establishing microstructurally-based relations between the material compositions and their cumulative properties [1-4]. The multifunctional topic of reference

Corresponding author: R.W. Armstrong, e-mail: rona@umd.edu

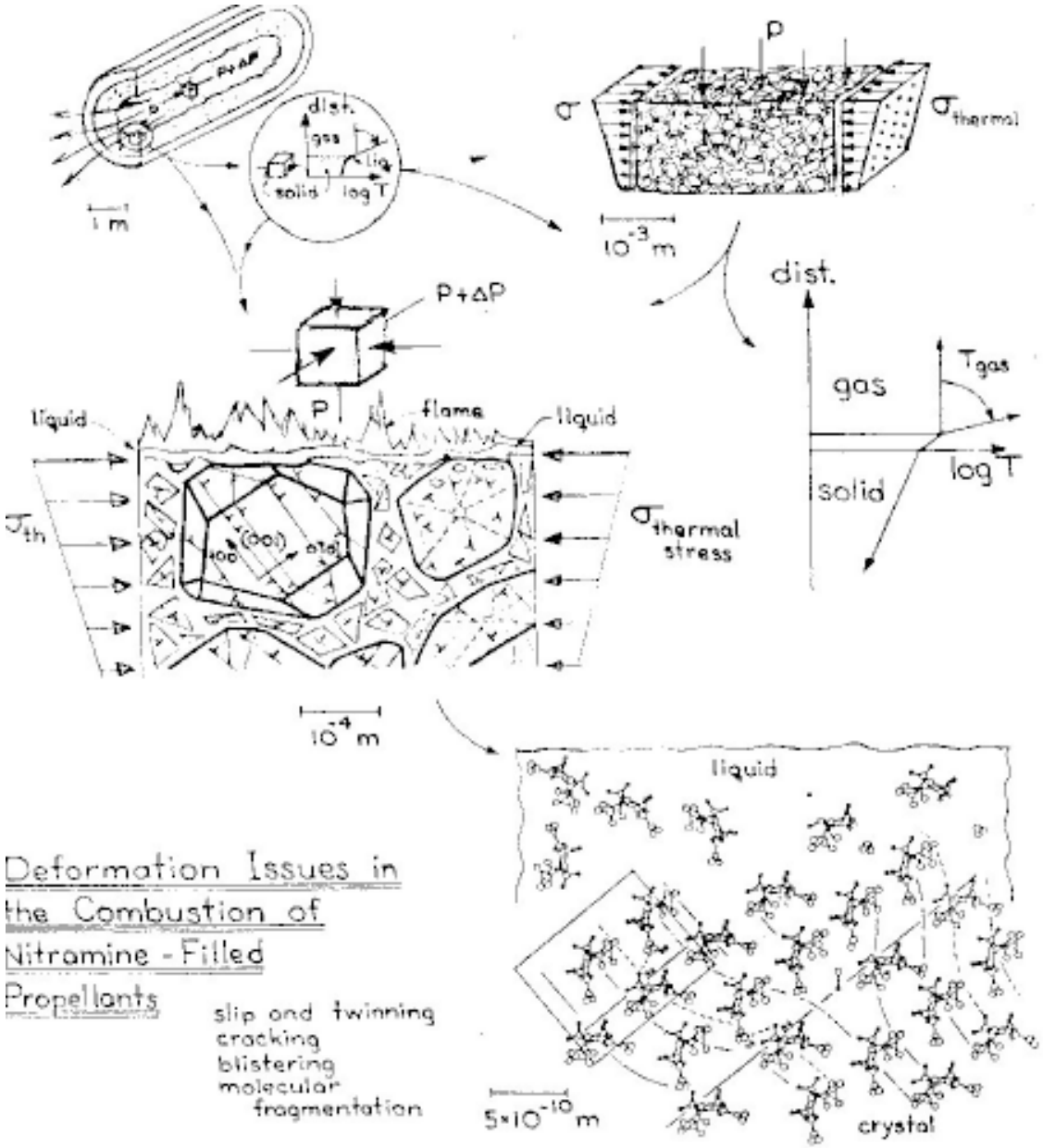


**Fig. 1.** Schematic picture of structural elements associated with propellant combustion.

[4] relates, in part, to the possible combination of energetic and structural load-bearing properties of a composite material being built into a single design package. As will be seen in the present report, the possibility is based in part on the achievement of advantageous properties on both considerations at nanometric dimensions of the composite ingredients [5]. In that regard, it's interesting that researches on the energetic materials themselves are often intertwined with studies of their detonation influences on the dynamic deformation properties of structural materials [6]. Such connection with the high strain rate properties of metals has been recently reviewed [7]. An historical note in that regard comes from B. Hopkinson, son of J. Hopkinson of split Hopkinson pressure bar (SHPB) fame, in contributing an early article on the topic of measuring the pressures generated in the detonation of high explosives or by the impact of bullets [8].

The occurrence of local thermal "hot spots" provides a historically-established mechanism for explaining the initiation of fast chemical decomposition within the various energetic materials; see, for

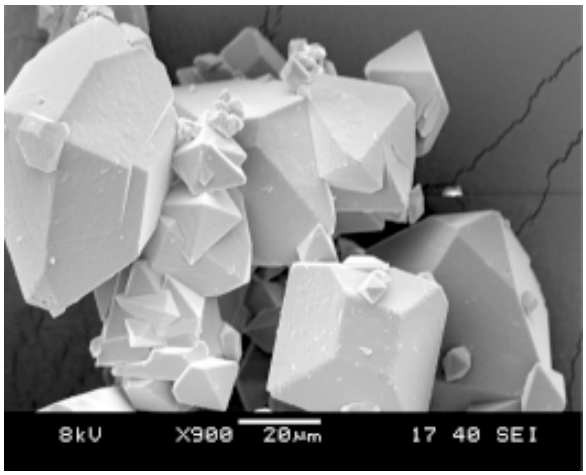


**Fig. 2.** Scanning electron microscope image of cyclotrimethylenetrinitramine (RDX) crystals.

example, reference [9]. The task of tracking such proposed hot spots is made more difficult by having to ferret through the complicated environment of energetic crystal responses occurring within a typical propellant formulation, as schematically depicted in Fig. 1, or within the more heavily filled constitution of an explosive formulation; see for example references [10-12], including in the last reference the formulation of a reactive metal system. And, for whatever energetic composite description is of interest, including that of a more heavily-filled plastically-bonded explosive (PBX), the decomposition behaviors, whether from direct thermal stimulus or under mechanical loading at the highest applied rates, including shock wave loading, are connected generally with variously modified Arrhenius-type thermal activation equation descriptions for either the measured or predicted temperature dependencies of the hot spot ignitions and their growth [13-20]. A principal concern of the present report is to relate to such considerations on two counts: (1) a dislocation defect role in providing localized sources for potential hot spot development; and, (2) the action of dislocation pile-up avalanches under mechanical loading in providing an important mechanism for initiation of fast chemical decomposition [21]. On this basis, special importance is attributed both to the role of dislocations in the original production of an energetic crystal as well as to the subsequent deformation-induced crystal responses.

## 2. CRYSTAL INGREDIENTS/ STRUCTURES

There is an important role of structural chemistry in understanding the nature of energetic crystal properties. Fig. 3 shows the crystal unit cell structure of cyclotrimethylenetrinitramine that is known by the substitute designation RDX and has an individual molecular formula $[CH_2 \cdot N \cdot NO_2]_3$. The bracketed manner of specifying the formula relates to the configuration of the molecule. Eight such RDX molecules, with individual covalent bonding between the carbon, C, hydrogen, H, nitrogen, N, and oxygen, O, elements, are relatively closely packed then within a molecularly-bonded orthorhombic unit cell with a Pbca crystallographic space group designation. The crystal lattice parameters are $a$ = 1.3182 nm, $b$ = 1.1574 nm, and $c$ = 1.0709 nm so having a unit cell volume of ~ 1.63 nm$^3$ containing 168 atoms [20]. Identification in the reported structural analysis of any smaller length for a typical covalent intramolecular bond distance, for example, for a labeled C3 – H5 bond length of 0.11 nm may be compared with a larger intermolecular bond distance, say, O1 – H2 of 0.25 nm length.

Two other energetic crystal materials to be especially referenced in the present article are: chemically-related to RDX, tetramethylenetetranitramine (HMX), $[CH_2 \cdot N \cdot NO_2]_4$; and, pentaerythritol tetranitrate (PETN), $[C \cdot (CH_2 \cdot O \cdot NO_2)_4]$. The Arrhenius-based hot spot model assessment mentioned above [9] lists RDX as being relatively stable thermally when compared to HMX and PETN that, in turn, are individually about equally less so but with PETN showing a stronger dependence of its critical hot spot size on temperature. The energetic crystal triaminotrinitrobenzine, (TATB), $[(NH_2) \cdot C \cdot C \cdot (NO_2)]_3$, that is relatively more stable mechanically in comparison to RDX, is an important ingredient of certain PBX formulations. Additional newer energetic crystals whose properties are being researched are CL-20, $2[C \cdot N \cdot NO_2]_3$, see [23], and FOX-7, $[(NH_2) \cdot C \cdot C \cdot (NO_2)_2]$, see [24,25]. Research continues on the design and synthesis of new energetic crystal structures and their thermo-mechanical response on the molecular scale [26-29].

Included among a number of other energetic composite ingredients whose properties are of interest, as to be described here, are so-called oxidizer crystals such as ammonium perchlorate (AP), $[NH_4 \cdot Cl_4]$, and the newer ingredient, ammonium dinitramide (ADN), $[NH_4 \cdot N \cdot (NO_2)_2]$. Aluminum, in polycrystalline form, is also an important additional

composite ingredient for energy release by oxidation. Recent research effort has been directed to the increased burning rate achieved for aluminum at nanoparticle sizes [30,31]. For comparison with the larger RDX unit cell volume, the well-known aluminum face-centered cubic (fcc) unit cell volume is ~ 0.064 $nm^3$ and contains four atoms. On balance, the mixture of covalent and molecular bonding among the elements in the RDX unit cell produces a lower material density of 1.8 $g/cm^3$ as compared with 2.7 $g/cm^3$ for aluminum. In general, concentrated mixtures of formulated ingredients are cast or pressed within a polymer binder matrix such as indicated in Fig. 1. The figure presents a schematic representation of the range in dimensional scales from the macroscopic level to the molecular scale within a hypothetical propellant material. As shown at the modeled burning interface of the polygonal energetic crystal in the figure, chemical decomposition occurs after melting ensues; and, this is experimentally demonstrated recently over a full range of compositions measured in the determination of an HMX-RDX phase diagram [32].

## 3. CRYSTAL CHARACTERIZATIONS

The energetic crystals themselves are generally produced by growth from supersaturated solvent solutions [33,34]. Fig. 3 shows an example batch of RDX crystals produced in the laboratory after a second crystallization from acetone solution of redissolved first-crystallized material [35]. The solution growth process is a standard method of crystal production, for example, as has been employed also in the obtainment of sucrose (sugar) crystals whose hardness properties were investigated as a comparative inert, or possibly energetic, material itself [36]. With regard to the later description to be given of the compaction properties of energetic material particle systems, mention is made that sucrose is also a model crystalline material that is employed in comparative pharmaceutical powder compaction studies.

A particular advantage of the solution-growth method is that different crystal morphologies may be produced with different solvents. The technique doesn't easily lend itself to the production of ultrafine crystal sizes except possibly by rapid expansion of supercritical solutions [37]. Other crystal growth methods of achieving finer-scale energetic crystal sizes are being investigated, for example, of membrane-assisted centrifugal crystallization or of evaporative crystallization [38]. Otherwise, finer

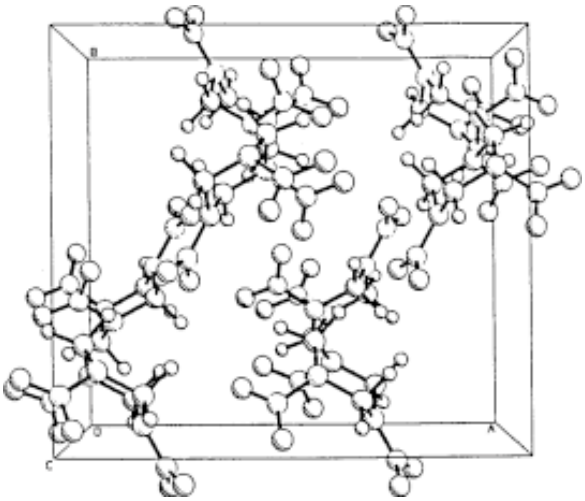

**Fig. 3.** RDX orthorhombic unit cell.

crystal sizes are achieved by mechanical comminution under protective environmental conditions [39]. And powder X-ray diffraction [40] is employed in most cases to evaluate the produced crystals so far as internal (dislocation) strains and porosity (also assessed through accurate density determinations) are important variables to be correlated with the crystal performances [41]. Association of voids and mechanically-induced hot spots is a long-standing research topic as exemplified in a recent report of necessarily ultra-small angle X-ray scattering being employed to monitor pore size distributions in TATB-based PBX-9502 materials and related formulations after being subjected to temperature cycling [42].

For research laboratory purposes of tracking individual or dislocation group characteristics, etch-pitting and X-ray diffraction topography methods have proved to be useful [21]. Electron transmission microscopy is generally not a useful method because of causing chemical decompositions. Figs. 4a – 4d show two constructions of modeled crystal growth configurations [43] and their match with optically etched [44] and X-ray (transmission) topographic measurements [45,46], respectively, obtained for sectioned RDX crystal specimens. The optically-identified traces of different {111} and {102} planes intersecting the viewed (001) planer surface of the RDX crystal in Fig. 4c relate directly to the crystal habit planes shown in Fig. 2. For example, the tabular crystal shown near the bottom-center of Fig. 2 exhibits four pyramidal planes of {111} type meeting at the planar (001) top facet

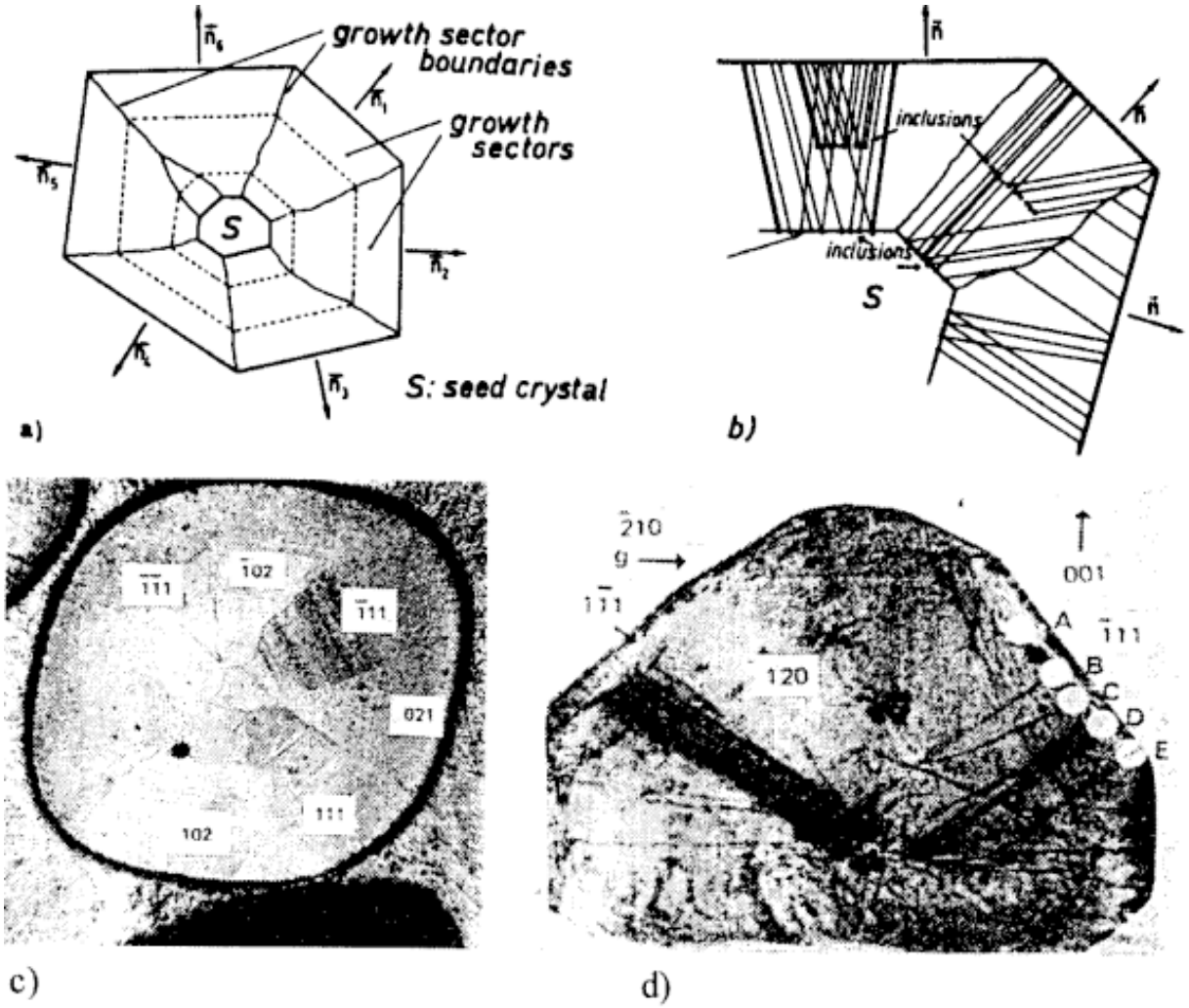


**Fig. 4.** RDX crystal growth sector and dislocation line structures.

and there is indication of a {102}-type facet trace at the top left crystal corner. The same crystal geometry is indicated for the edge-on view of the larger tabular crystal shown in the top-left corner of Fig. 2. Thus the identified planar traces in Fig. 4c are indicative of the sequential surface positions occupied by the RDX crystal during its growth and are distinguished apparently in the crystal etching process of Fig. 4c because of extremely small variations in solute concentrations incorporated within the crystal during growth.

Very often, the initial crystal nucleation is known to occur on an inclusion or intentional “seed” particle, as indicated schematically in Fig. 4a. Fig. 4c gives such indication within the RDX crystal. The internal strains sometimes generated by such seeding mechanism have been imaged in several RDX X-ray topographic images [47]. Also of interest in relation to the dislocation line structures shown in Fig. 4d are the crystal defect indications exhibited at the top surface and corner of the larger tabular crystal viewed edge-on in Fig. 2. The steeply inclined (001) planar top is seen to involve a partial twist about its normal [001] direction that must correspond to an internal defect with displacement vector along the same [001] direction, that is the smallest repeat distance for a dislocation Burgers vector in the crystal lattice. Generally but not always, such smaller vectors are associated with the defect line characteristics modeled in Fig. 4b for dislocation-associated crystal growth. The mismatch of growth facets at one corner of the larger crystal is seen to be associated with the formation of another crystal appendage. Other X-ray topographic results reported for dislocation distributions within solution-grown RDX crystals have indicated

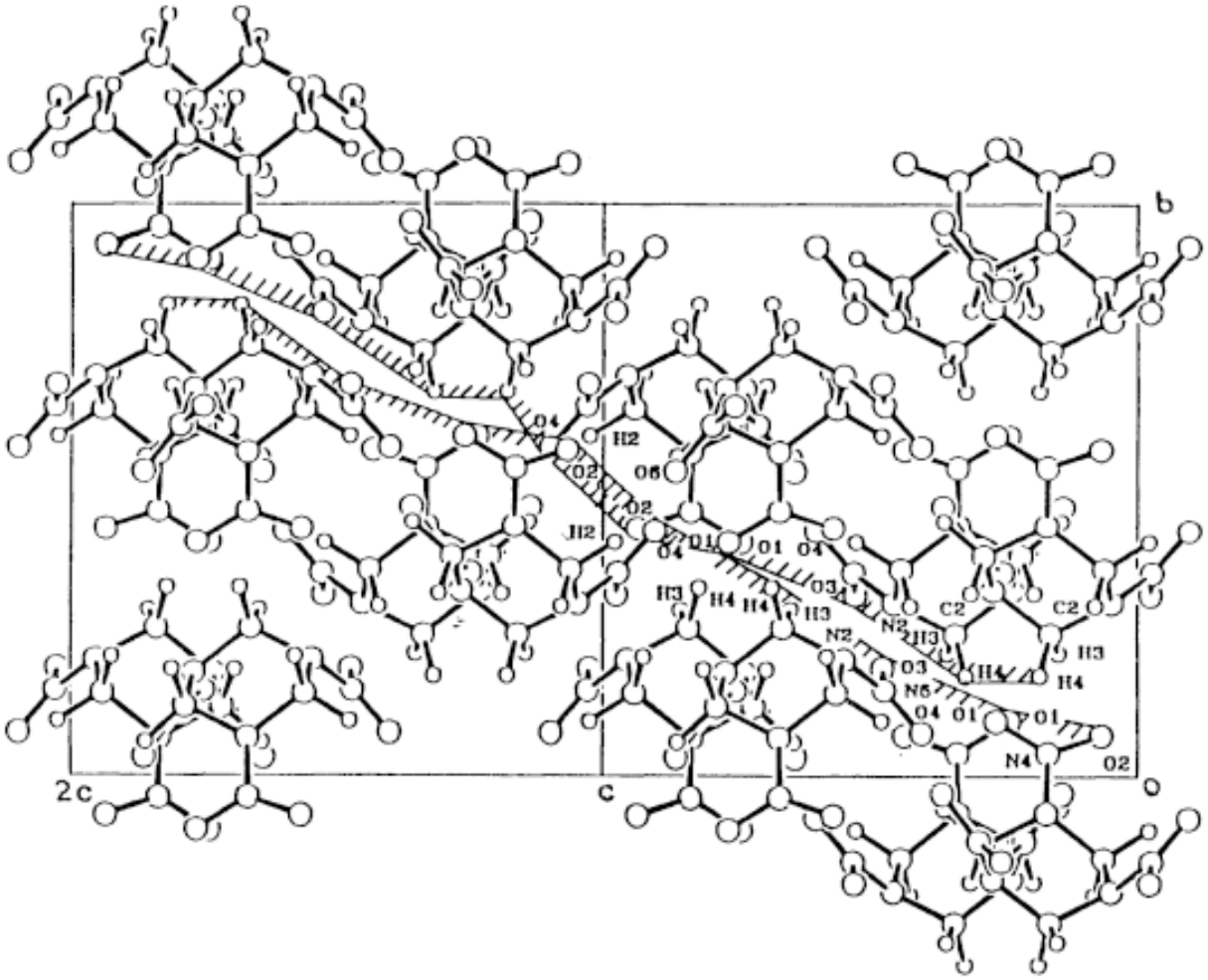


**Fig. 5.** Intermolecular blockages for shear in a [100] direction across the (02-1) plane in RDX.

that the crystals contain relatively low dislocation densities and have a variety of dislocation line directions and Burgers vectors [48,49], perhaps not unexpected for a relative weakly-bonded molecular crystal structure.

## 4. EXPERIMENTAL MECHANICS

The relative brittleness of energetic crystals has been a main factor leading to the use of indentation hardness testing as a method of evaluating their plastic deformation behaviors and, likewise, has led to the use of indentation fracture mechanics (IFM) as a method of assessing the material cracking behaviors. The susceptibility of the materials to initiation of fast chemical decomposition under impact has been established in laboratory tests by use of calibrated drop-weight tests, generally, of loose piles of the crystals. Higher loading rate shock wave testing, via explosive loading or accelerated plate impacts or by means of impacting with laser beams, has been applied to crystals while also their decompositions are monitored with a variety of physico-chemical test diagnostics; see for example [50,51]. The material deformations and cracking behaviors when subjected to granular compaction under controlled conditions are also of interest for both research and manufacturing purposes.

### 4.1. Indentation hardness properties

In laboratory experiments, dislocation etch-pitting applied to microindentation hardness impressions put into RDX crystal surfaces led to the observation of very limited spreading of the dislocations having occurred in comparison with the well-established, more extensive, patterns of strain ro-

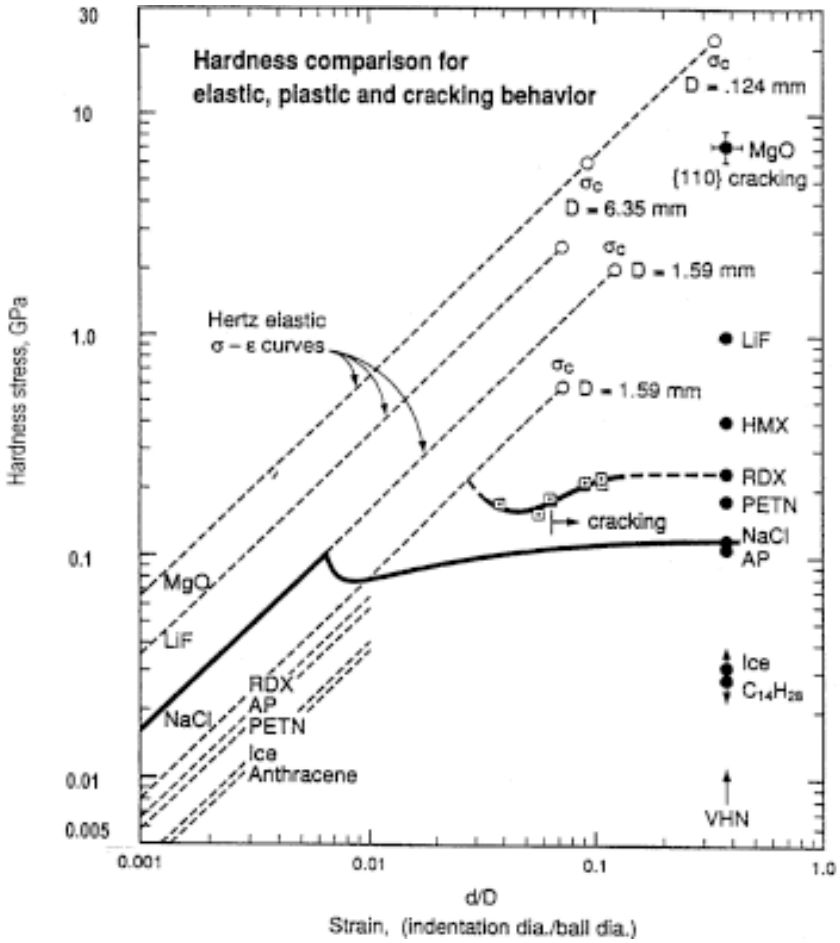


**Fig. 6.** Hardness stress – strain description for elastic, plastic, and cracking behaviors.

settes observed at etched microindentations in LiF [52]. Also, the observation of slip on {021} planes was identified at the RDX indentation sites [53] in extension of other pioneering etch pit observations [33]. The {021} slip system result was confirmed in accompaniment of the reported X-ray topographic results mentioned above [49] and was included in a further analysis of operative slip systems at RDX hardness indentations [54]. On the molecular lattice scale, mutual blockages to slip across the {021} planes in an [001] slip direction were shown to be caused by interactions of out-cropping molecular appendages, as modeled for RDX in Fig. 5 at the sites of the partially labeled atomic elements. The interactions were associated with reported nitroso-compound formations that have been detected in drop-weight impacted crystals tested just below the initiation drop-height [55] and also were detected in combustion residues [56]. Thus, the etch-pitting observations made on RDX crystals provided a first indication of dislocation displacements being hindered in a particular manner characteristic of complex molecular interactions occurring within the rather more complicated energetic crystal lattices.

Fig. 6 shows a hardness stress-strain method of analysis that provides for further comparison of elastic, plastic and cracking behaviors among energetic and other material crystal types [57]. In the figure, the plastic hardness stress, $\sigma_\mu$, is specified for a ball indentation as the indenter load, *W*, divided by the surface projected contact area of the residual indentation having a real or effective crater diameter, *d*. The hardness strain is the indentation diameter divided by the ball diameter, *D*. The dashed lines sloping steeply upwards in Fig. 6 from the lower left edges are Hertzian elastic line dependencies for which the *d* values are taken as the elastic contact diameter in the expression

$$\sigma_E = (4/3\pi)\left[\left\{\left(1-\nu_b^2\right)/E_b\right\} + \left\{\left(1-\nu_s^2\right)/E_s\right\}\right]^{-1}(d/D). \quad (1)$$

In Eq. (1), $\nu_b$, $E_b$ and $\nu_s$, $E_s$ are the Poisson's ratio and Young's modulus for the ball and specimen, respectively. The reciprocal factor in square brackets on the right side of Eq. (1) is normally replaced by an effective modulus, $E_r$. Separate from the elastic predictions, a number of crystal plastic hardness values are shown in the figure as filled circle points vertically distributed along the ordinate scale at an effective value of ($d$/$D$) = 0.375, as determined for diamond pyramid or Vickers hardness (test) numbers (VHN). The crystal materials that are listed for these hardness values include, in addition to the crystals identified thus far, MgO, NaCl, ice, and anthracene. As shown in the figure, an increasing hardness is determined for the materials of present interest in the order of AP, PETN, RDX, and HMX. For NaCl, the solid elastic loading line and connected plastic flow curve were determined in a continuous loading test. Such elastic loading behavior is more easily demonstrated in modern nanoindentation hardness tests, for example, as reported for sucrose crystals that were investigated for comparison with energetic crystal properties [58]. The series of open square points shown for an RDX crystal were measured by means of a microindentation hardness tester fitted with a 1.59 mm diameter steel ball indenter.

In Fig. 6, the open circle points specified at particular $D$ values along the dashed Hertzian lines are modeled hardness stresses for cracking, $\sigma_C$, computed in accordance with the indentation fracture mechanics (IFM) expression:

$$\sigma_C = \left\{4E_s\gamma/\left[\pi D\left(1-\nu_s^2\right)\cdot\left(\kappa_1^2+\kappa_2^2\right)\right]\right\}^{1/2}(d/D)^{-1/2}, \quad (2)$$

in which $\gamma$ is the true surface energy and the numerical factor $(\kappa_1^2 + \kappa_2^2) = 2.5\cdot10^{-5}$ was taken as originally reported [59]. The highest average hardness (closed circle) point in Fig. 6 was determined for a number of MgO crystal indentations made on (001) plane surfaces. The $D$ = 0.124 mm label at the highest value of $\sigma_C$ on the dashed MgO elastic loading line was determined as the equivalent (average) ball size for the actual diamond pyramid indentation measurements that are shown. At such indentations on (001) surfaces of MgO crystals, dislocation pile-ups are known to produce distinctive, crystallographically-defined, cracking patterns [60]. Very importantly, the dislocation pile-ups are shown in the figure to initiate cracking at a significantly lower hardness stress than that predicted on an IFM basis and, even so, the cracking occurs on {110} cleavage planes that require a higher surface energy than the otherwise favored (001) planes. The lowest $\sigma_C$ value marked at $D$ = 6.35 mm on the MgO Hertzian line, nevertheless, demonstrates the reduction in predicted IFM cracking stress occurring in accordance with the inverse square root of $D$ factor in the coefficient of the ($d$/$D$)$^{-1/2}$ strain dependence in Eq. (2).

The cracking specified to occur for RDX at the larger strain, open square, measurements in Fig. 6 are also positioned below the predicted $\sigma_C$ value for a $D$ = 1.59 mm ball as designated at the terminal point of the Hertzian elastic line. Here too, the measured hardness for cracking is lower because of a same dislocation pile-up-induced cracking reason although very probably needing only a small number of dislocations in the pile-ups. Thus, the difference in RDX stress levels between the cracking-associated plastic hardness and the predicted IFM-determined cracking stress is shown to be significantly smaller than that shown for the corresponding separation of stresses for NaCl, which is not known to be an exceptionally ductile material. Such observation is indicative of a lesser range in stress being available in RDX for any influence of dynamic loading. A further comparison of the RDX and NaCl hardness results shows that NaCl is elastically stiffer, as expected on the basis of its stronger ionic bonding, while RDX is plastically stronger, because of its lattice hindrance to slip and, also, is more cleavage prone because of its relatively lower surface energy [21]. Other comparisons have been made between RDX and MgO crystals in terms of an IFM predicted $c^{3/2}$ crack size dependence of $\sigma_H$, or $c^2$ dependence in accordance with cracking being controlled by the hardness value [61]. The indication for RDX of the measurements fitting the latter dependence is in agreement with crack growth being controlled by the limited extent of plasticity occurring at the crack tip. The same conclusion had been reached in an earlier assessment of the IFM measurements reported for the RDX cracking behavior [62].

Additional evidence for plastic flow being a principal cause of crack formation in both energetic and ionic crystals was demonstrated for plasticity-induced cracking observations made for diamond pyramid hardness indentations put into AP crystal surfaces [63,64]. The AP results in [63] included X-ray topographic evidence, analogous to the case for {110} cracking in MgO, of substantial internal

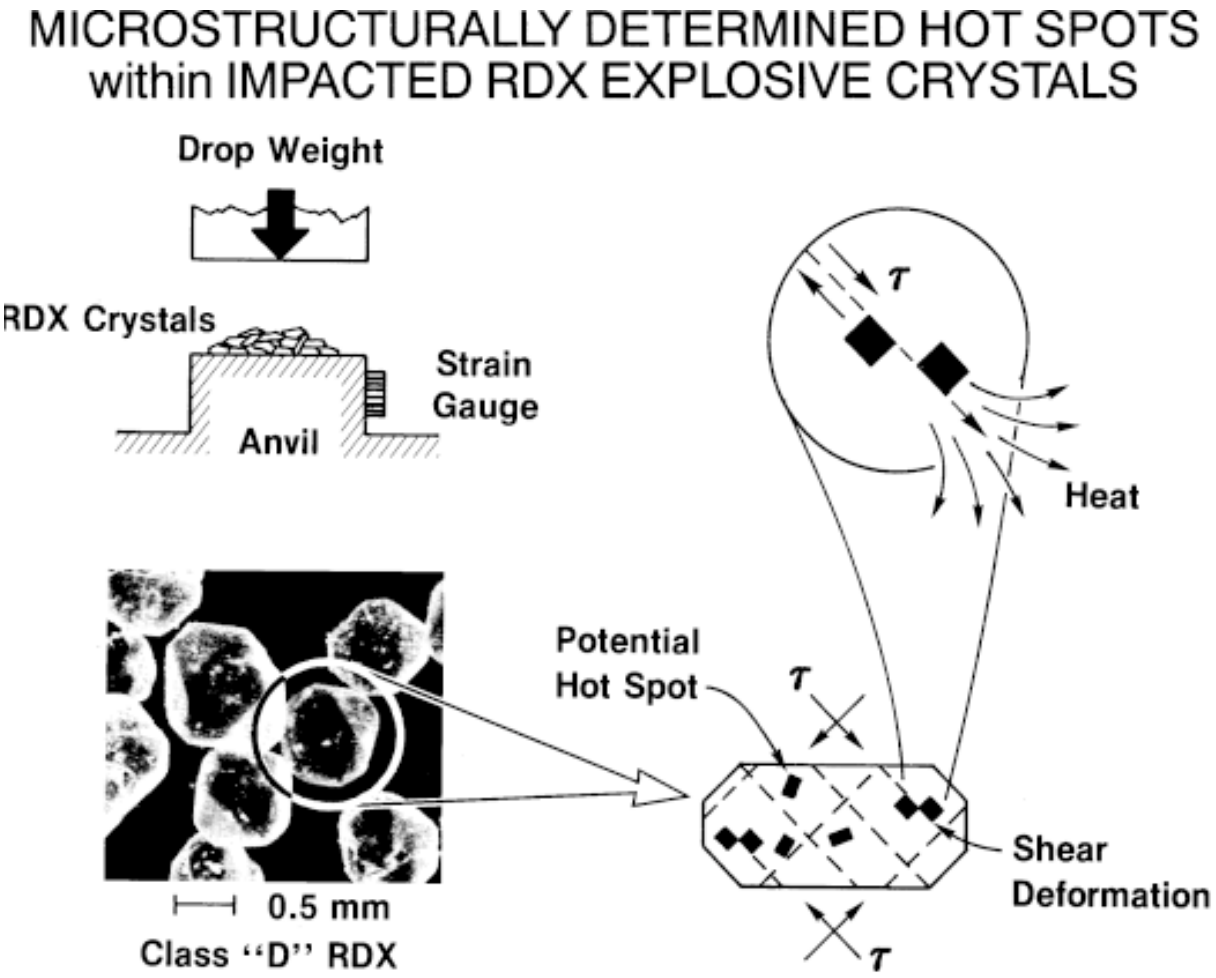


**Fig. 7.** Schematic drop-weight impact test of RDX crystals and hot spot generations.

lattice strains associated with locally-identified slip band stress concentrations that produced cracking. In [63], a hardness measurement of 265 MPa was obtained for the newer ADN oxidizer crystal. The value is greater than that for AP shown in Fig. 6 and is nearer to the level shown for the RDX measurements. In [64], strikingly imaged terraced structures are shown at dislocation etch pits imaged by atomic force microscopy on the (210) surface of an AP crystal. The terrace structures are very likely a finer scale manifestation of the layered-type growth structure features revealed in Fig. 4c for an RDX crystal [44].

## 4.2. Impact properties

A schematic representation of a drop-weight impact test is shown in Fig. 7 as applied to measuring the impact sensitivity of loose piles of energetic crystals. The figure includes a sample view of RDX crystals and, also, a model interpretation of crystal lattice shearing for development of hot spots leading to initiation of the impacted crystals [65]; note the 1-2 mm size of the crystals in Fig. 7 compared to the ~50 micron-sized crystals shown in Fig. 2. More detailed descriptions of drop-weight impact testing machines have been reported [66,67]; in the first case involving optical recording of the material deformation and cracking behaviors and, in the second case, also including results obtained on a number of explosive materials tested in a ballistic impact chamber (BIC). Fig. 8 shows a compilation of early results reported for the drop-weight impact height for 50% probability of initiation, $H_{50}$, as a function of the average size of individual crystals within the pile [68,69]. As observed for the data included within the limits of the dashed inset in the

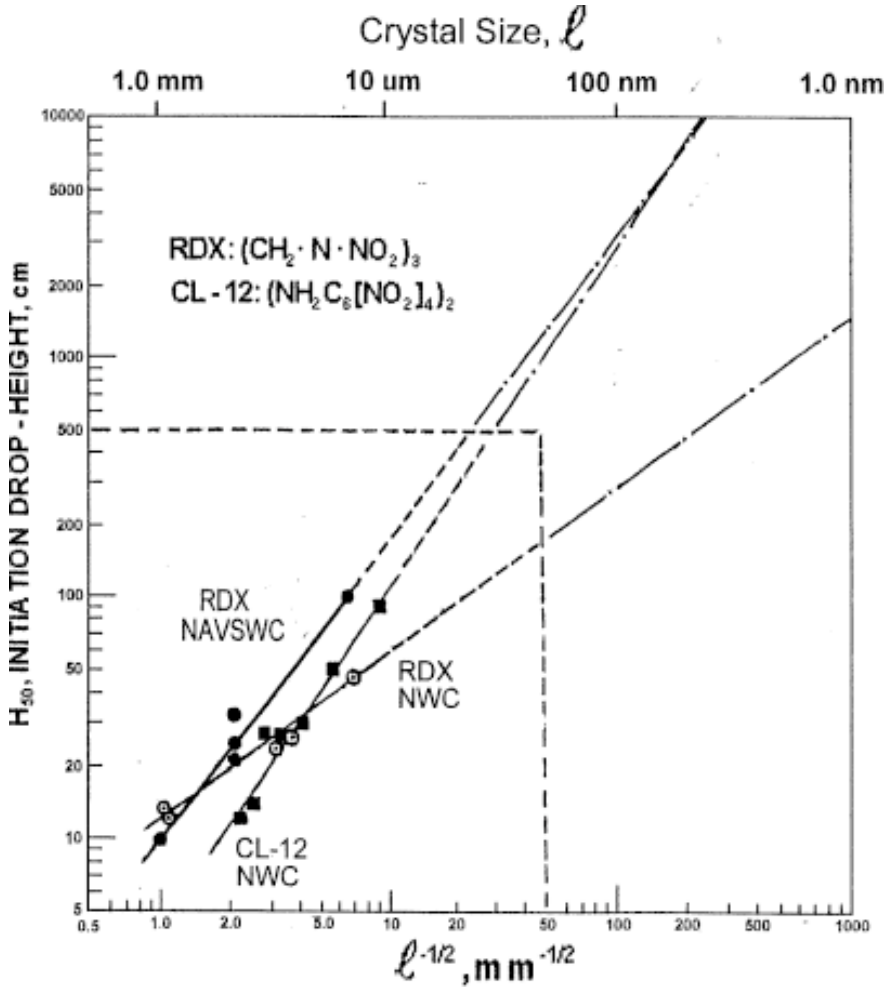


**Fig. 8.** Crystal size dependence for initiation of RDX and CL-12 in drop-weight impact tests.

figure, a strong dependence of $H_{50}$ on crystal size is obtained; for example, an order of magnitude increase in $H_{50}$ from 10 to 100 cm is produced for a crystal average size reduction from 1.0 to 0.01 mm, while also indicating a reciprocal square root dependence of $H_{50}$ on the crystal size. The larger dimensional extension of the graph comprising Fig. 8 was constructed for connection with current research emphasis on measuring energetic crystal properties at nanometric crystal sizes. Determination of a drop-weight height in excess of 100 cm has been reported for RDX crystal diameters in the range of 110 to 300 nm, as referenced above to be obtained by the method of rapid expansion of a supercritical solution of RDX in carbon dioxide [37].

Other methods of researching the impact-initiated properties of formulated composite materials include: Taylor-type cylinder impact tests [70], as employed for characterizing the strength properties of structural metals and alloys; split-Hopkinson pressure bar (SHPB) or hybrid-SHPB tests [71]; ballistic penetrations [72], as mentioned above for the historical article [8] of Hopkinson; and, especially, shock-induced impact tests achieved by explosive detonation-type gap tests or gas-gun- or laser-launched projectiles [73]. For example, the last-mentioned testing procedures of gap tests and laser launched flyer plates were applied to evaluation of the shock sensitivity for PETN crystals of ~1 and 180 micron sizes pressed to 90% theoretical maximum density. Opposite size-dependent crystal sensitivity results were obtained with the two test methods. The smaller particles were more shock sensitive in the laser impact results and less shock sensitive in the gap tests. The results appear to be particularly important because of the suggested relationship made here of the neat crys-

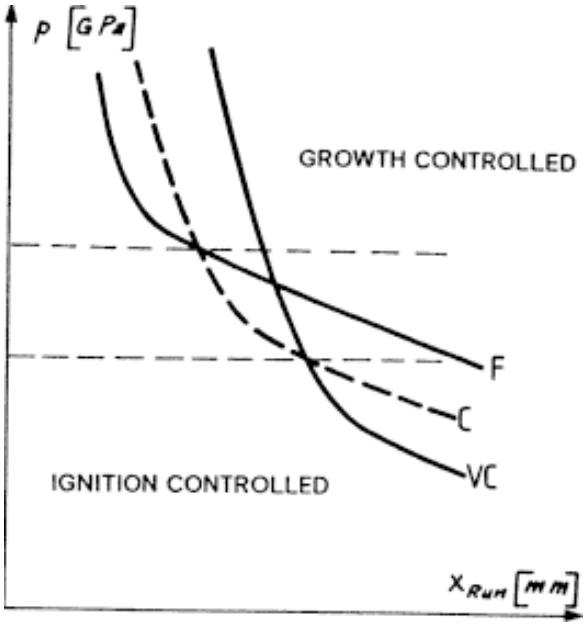


**Fig. 9.** Schematic size dependence of fine (F) coarse (C), and very coarse (VC) crystal ingredient influences on the run-to-detonation distances as a function of required shock-induced decomposition pressures.

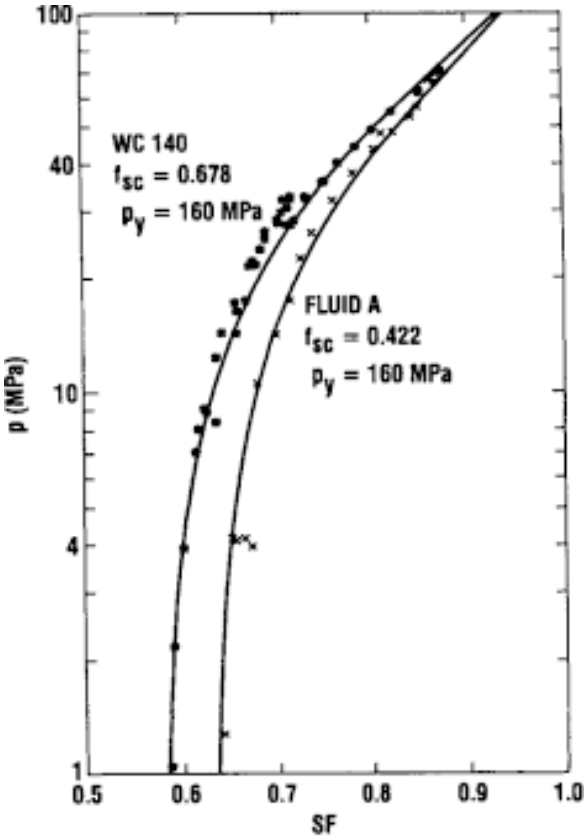


**Fig. 10.** Experimental and modeled granular compaction pressures for two commercial powder materials as a function of solid fraction (SF) as modeled with a specified fraction of particles in a simple cubic lattice, $f_{sc}$, and a mean-hardness-determined particle-to-particle contact pressure, $p_y$.

tal results being analogous to pioneering flyer plate test results made on cast 70% RDX/30% polyurethane PBX formulations containing individual monomodal RDX particle sizes ranging between 6 and 428 microns; see the schematic Fig. 9 for the different shock pressure dependencies on the run-to-detonation distances for different fine (F), coarse (C), and very coarse (VC) crystal sizes [74]. As argued in the earlier PBX case for discriminating between proposed control by ignition of hot spots within individual particles at low pressures as compared with control at high pressures by growth of reaction through hot spot coalescence, the difference in PETN results were attributed to the restricted growth of hot spots in the narrower pulse (and higher pressure) laser tests as compared to initiation control in the longer pulse (and lower pressure) gap tests. The (crystal or) particle size effect described in Fig. 9 has been investigated more recently in development of an “extended statistical hot spot model” description leading to predicted hot spot ignition and growth dependences for a neat particle-sized material in which the hot spots are initiated at particle-to-particle contact points and the thickness of a coalesced hot spot region is taken into account for the hot spot growth mechanism [75]. Easier initiation in gas-gun experiments of reactive Al/PTFE (polytetrafluoroethylene) formulations has been quantitatively demonstrated for the composite material containing smaller aluminum particles [76].

The employment of laser-induced initiation behaviors deserves particular attention for analogous use of the method to produce local melting/damage sites for examination in individual crystal studies, for example, of AP crystals [63,77]. Aquarium-type shock-induced chemistry results have been obtained after pre-test microindentations had been put into the crystal surfaces to serve as potential damage sites [78-80]. For an AP crystal, both nanosecond and picosecond laser-pulse-induced cleavage-type cracking observations were reported in association with sub-surface chemical decomposition sites produced below an (001) crystal sur-

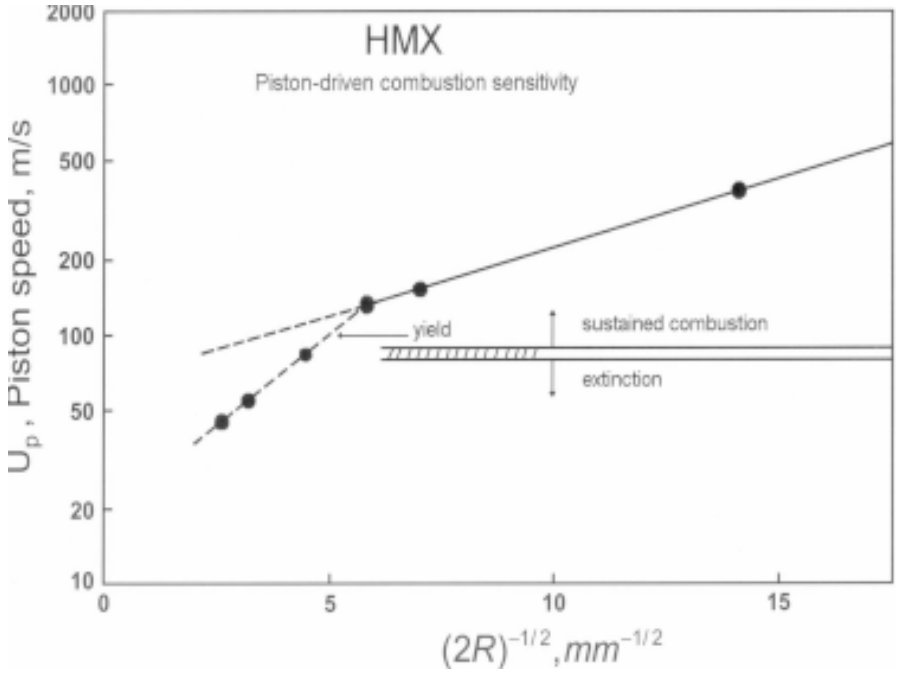


**Fig. 11.** Reciprocal square root of crystal diameter dependence of piston speed modeled to assess the sensitivity for combustion of HMX crystals.

face impacted with a Nd/YAG-generated beam. Sufficiently high temperatures were reached at the laser-impacted crystal regions to cause the AP orthorhombic-to-rocksalt structure-type phase transformation and to cause crystallographically-defined cracking on the (210) and {100} planes of the respective structures. X-ray photoelectron spectroscopy was applied to detect chlorine as a decomposition product. Scanning electron and atomic force microscopy observations led to association of chemical decomposition with the micron-scale, sub-surface, hot spot sites. A dislocation reaction model basis was developed to show local dislocation-generated stress enhancement for chemical reaction. With regard to the role of cracking in certain energetic crystal initiations, a statistical crack mechanics approach, based on the well-established theory of penny-shaped cracks, has been proposed for wider application to explaining the shock-induced impact sensitivity behaviors of both propellant and high explosive materials [81].

## 4.3. Granular compaction

As might be imagined from the mention in Section 3 above of mechanical pressing operations done to manufacture energetic material formulations and for the shock-induced hot spot behavior of pressed PETN crystals [73] mentioned in the immediately above Section 4.2, crystal compaction is of interest both for practical and research-driven purposes. Considerable research effort has been devoted to adapting the knowledge gained from powder metallurgical [82] and pharmaceutical [83] experience to that for compacting energetic materials but with added concern, connecting to the latter industry, for the material brittle cracking behaviors. Such pharmaceutical connection has been mentioned in obtainment of recent nanoindentation test results reported for sucrose as a model brittle molecular crystal [58]. Elegant nanoindentation test results were reported also for AP in [64]. The hardness of such materials might be imagined to be intimately connected with their compaction behaviors as well. Fig. 10 shows compaction results reported for two commercial energetic material formulations and as fitted in each case with a model description of the compaction process; FLUID A is a solid material [84]. In the figure, the compaction model parameter, $f_{sc}$, is determined as the mass fraction of simple cubic lattice site positions distributed among presumed simple cubic and face-centered cubic particle organizations; and, $p_y$ is the mean hardness stress applicable at the deforming particle-to-particle contacts.

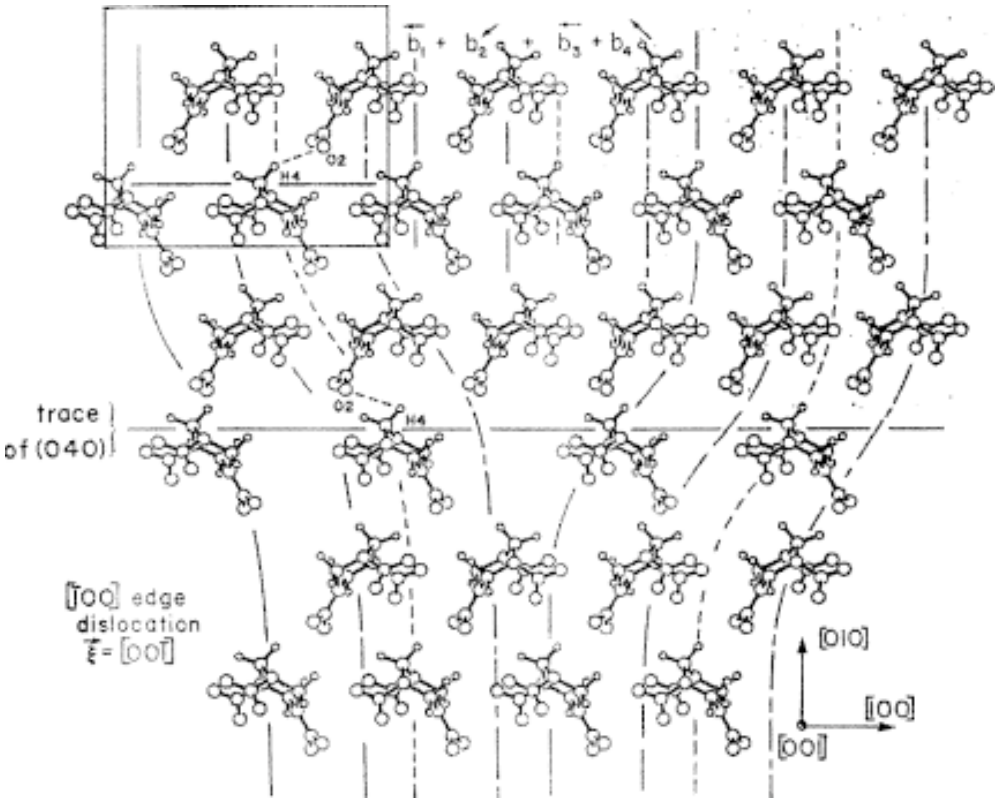


**Fig. 12.** Schematic picture of a [-100] edge dislocation on the (040) plane in an RDX crystal projection having a (002) planar depth as shown for the framed rectangular unit cell.

In [84], experimental results were reported also for the quasi-static compression of different crystal sized HMX particle beds. In another investigation employing the same results, a model description was developed for the particle size influence on combustion through plasticity-induced hot spots developing at the particle-to-particle contacts and relating to the material contact hardness properties [85]. Fig. 11 shows the modeled results as later analyzed on a reciprocal square root of particle diameter basis [57] consistent with the display of the crystal sensitivity measurements shown in Fig. 8 [69]. In construction of the figure, the modeled piston velocity was taken to be proportional to the logarithm of the plastic strain rate, as will be described below for conventional dislocation mechanics based constitutive equation behaviors. The break in the linear dependence, distinguishing between sustained combustion and extinction, is seen to occur approximately at the point of full plastic yielding behavior of the particle bed. The results demonstrate again a greater resistance to initiation of decomposition, this time for combustion, at smaller particle sizes.

## 5. DISLOCATION MECHANICS

Thus far in the information covered above, correlations have been indicated for a number of described energetic material properties and various aspects of the material dislocation behaviors, for example, as centered on the several levels of: (1) individual dislocation characterizations; or (2) the dislocation pile-up avalanche model proposed to explain hot spot formations and crystal (particle) size effects; or (3) the related consideration of dislocation pile-up-induced cracking behaviors.

### 5.1. Dislocation characterizations

Fig. 12 shows a schematic (001) plane representation of an edge dislocation with [100] Burgers vector on an (040) slip plane in the orthorhombic RDX crystal lattice [86]. The (010) slip plane had been identified in the referenced pioneering etch pit study [33]. The dislocation is naturally fully capable of cross-slipping onto the (021) plane that has been described with respect to promoting the nitroso-compound formation detected in drop-weighted impact specimens falling short of full ini-

**Table 1.** Comparison of dislocation and cracking parameters.

| Material | Dislocation Strain Energy ($E_{\perp/p}$), J | $\left(\frac{E_{\perp/p}}{\Delta H_{f/m}}\right)$ | Peierls-Nabarro Stress ($\tau_p$), N/mm$^2$ | ($\tau_p/G$) | Dislocation Stress Intensity ($k_s$), N/mm$^{3/2}$ | ($k_s/G$), mm$^{1/2}$ | (g/$Gb$)$^{1/2}$ |
|---|---|---|---|---|---|---|---|
| RDX | $6.3\cdot10^{-19}$ | 12 | 580 | 0.077 | 7.7 | $10\cdot10^{-4}$ | 0.066 |
| PETN | $3.3\cdot10^{-19}$ | 4.0 | 394 | 0.073 | 5.9 | $11\cdot10^{-4}$ | 0.070 |
| AP | $1.2\cdot10^{-19}$ | —— | 1200 | 0.162 | 6.3 | $8.5\cdot10^{-4}$ | 0.088 |
| LiF | $0.9\cdot10^{-19}$ | 2.1 | 3100 | 0.050 | 29 | $4.6\cdot10^{-4}$ | 0.14 |
| MgO | $2.4\cdot10^{-19}$ | 1.9 | 8000 | 0.054 | 70 | $4.7\cdot10^{-4}$ | 0.17 |

$$E_{\perp/p} = \left(Gb^2\Delta\xi / 4\pi\bar{\alpha}\right)$$

$$\tau_p\left(=\tau_{p\cdot N}\right) = \left[2G/(1-\nu)\right]\exp\left[-\pi d/(1\cdot\nu)b\right]$$

$$k_s = \left(\pi G b^{1/2} / 4\bar{\alpha}\right)$$

tiation behavior [55]. From a most basic dislocation mechanics evaluation, the total dislocation energy, $E_T$, is specified for unit molecular length, $\Delta\xi$, of dislocation line as

$$E_T = \left(Gb^2\Delta\xi / 4\pi\alpha\right)\ln\left(R / r_0\right) + E_C. \quad (3)$$

In Eq. (3), $G$ is the shear modulus, $b$ is the dislocation Burgers vector (displacement), $\alpha$ is $(1 - \nu)$ for an edge dislocation or 1.0 for a screw dislocation or a (reciprocal) average value for a mixed dislocation, $R$ is an outer cut-off radius, $r_0$ is the dislocation core radius, and $E_C$ is the non-linear elastic dislocation core energy.

Table 1 provides in the first column after the material identifications a comparison among several materials of the bracketed coefficient of the logarithmic factor in Eq. (3). And the adjacent column presents the same coefficient divided by the heat of formation per molecule. Comparison of the different material numbers shows that dislocations in RDX and PETN have relatively higher self-energies, consistent with relatively low dislocation densities being measured by etch-pitting and X-ray topography. The result is a consequence of the relatively large Burgers vector and unit line length factors out-weighing a relatively lower shear modulus. The dislocation line energy in Eq. (3), particularly including the anisotropy of $G$ values, is proposed to be an important factor along with $b$ in determining the line orientations of dislocations participating in such crystal growth processes as indicated in Figs. 4b and 4d [43].

The dislocation core energy and radius, $r_0$ in Eq. (3), are associated with another interesting feature for molecular crystals and other materials exhibiting large Burgers vectors. For them, an early dislocation model computation showed that a lower energy condition was favored by having a cylindrical hole or liquid core running along the dislocation line [87]. Recent calculation has been given for the hole possibly having an elliptical shape [88]. The presence of water in the dislocation cores of sucrose crystals has been employed to explain an enhancement of their electrical conductivity [89]. An early report was made of solute-containing inclusions occurring during the growth of RDX crystals [90] and, more recently, gas bubbles, sometimes elongated into channels, have been reported in a careful study of the growth characteristics of (organic) benzil crystals [91]. Hollow “micropipes” have been imaged at surface intersections for silicon carbide crystals and have been proved *via* X-ray topographic examination to be centered on dislocation lines [92]. Related nanopipe influences have been described for epitaxial layers of gallium nitride grown onto sapphire crystal surfaces [93]. Such special dislocation core considerations are particularly important for energetic crystals because

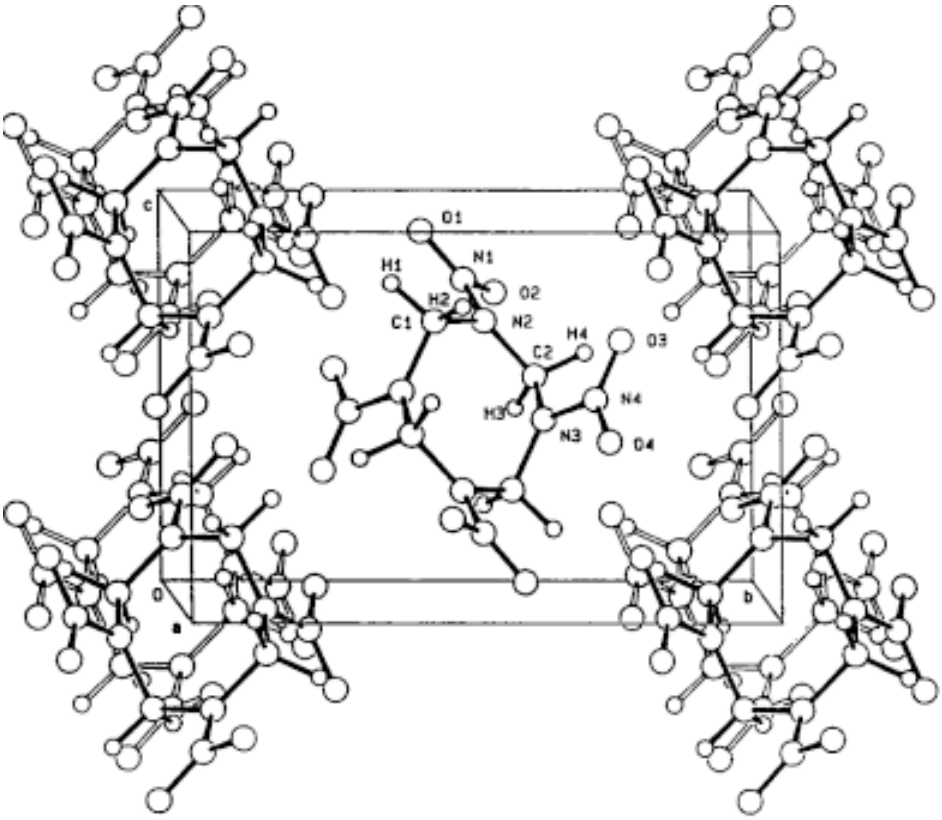


**Fig. 13.** The monoclinic unit cell of β-HMX (cyclotetramethylenetetranitramine).

of their relatively low surface energies, as has been mentioned [62] and will be discussed with regard to the cleavage cracking behaviors too.

The Peierls-Nabarro (P-N) stress evaluations identified in Table 1 are those defined on a continuum mechanics basis for which d is the slip plane spacing. On such basis, that can only be considered very approximate because of the molecular complexity pointed out for the modeled shear-type displacements occurring for slip in an energetic crystal lattice, for example, for RDX in Fig. 5, both it and PETN have relatively higher P-N stresses when normalized with regard to their shear moduli. A pioneering molecular dynamics calculation has been described [94] for an edge dislocation in anthracene that is plastically relatively soft, as indicated on the basis of the plastic hardness comparison demonstrated in Fig. 6. Other analysis of the relative difficulty presented by intermolecular interactions of the type mentioned for Fig. 5 had been described earlier for different slip systems in anthracene [95]. More recently, a molecular dynamics description has been developed for anthracene so as to distinguish on a model basis between hydrostatic and non-hydrostatic influences in compression tests [96].

The deformation behavior of HMX, though not included in Table 1, is of special interest because of twinning being the main response in this case to mechanical loading. Fig. 13 is an illustration of the HMX monoclinic unit cell for the structure of the ambient temperature β-polymorph, among three other polymorphs occurring at higher temperatures and pressures [97]; and, Fig. 14 provides a model description of the (101)[10-1] twinning shear of lattice points. In general, the fixed shear strain characteristic for twin nucleation requires that local stress concentrations from micro-slip of dislocation pile-ups be involved; and, consequently, for polycrystalline materials, a relatively strong grain size dependence is observed for the applied twinning stress [98]. Such pre-twinning slip is indicated to be a minor consideration for HMX, however, because of the twin occurrence being reversible at small strains [99], as is documented for the classic case of deformation twinning in calcite crystals. The

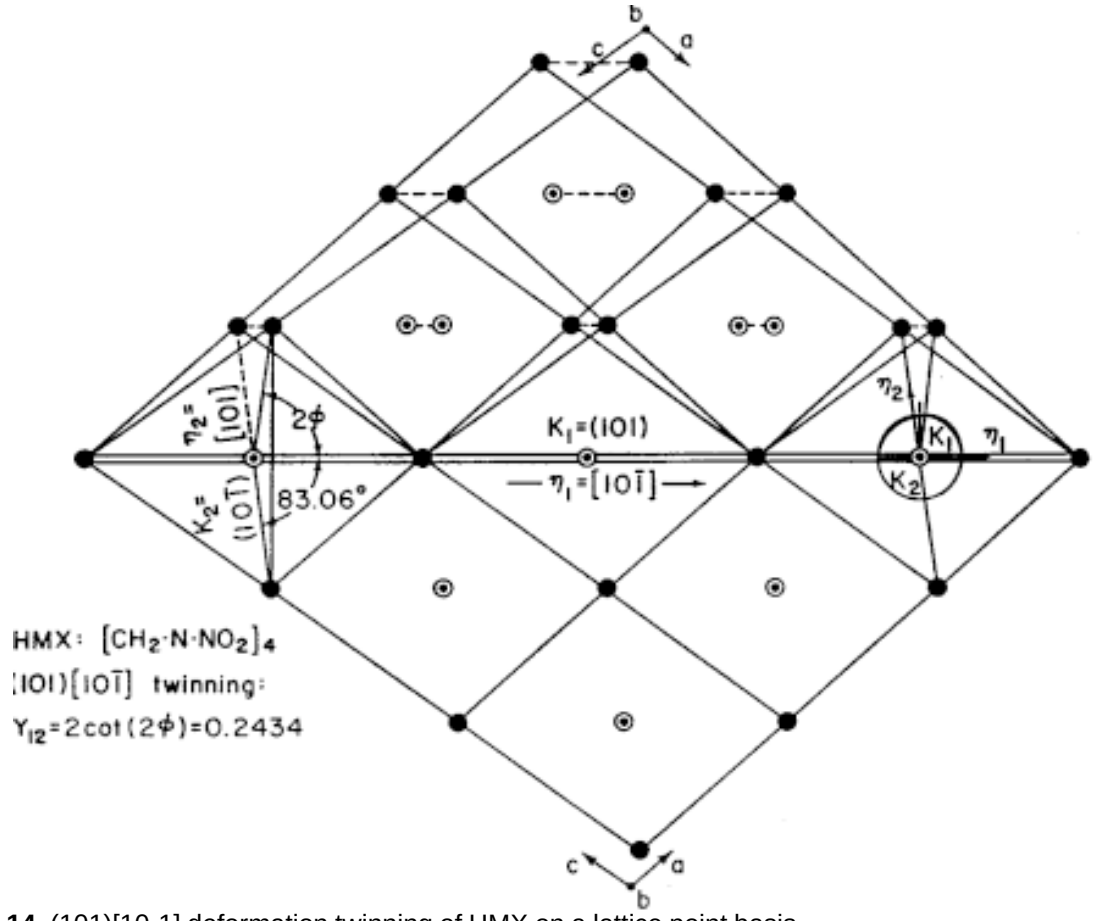


**Fig. 14.** (101)[10-1] deformation twinning of HMX on a lattice point basis.

comparison of slip being dominant in RDX as compared to twinning being dominant for its chemically related counterpart has been attributed to the flexibility of the larger HMX molecule [100], in agreement also with the changed shape of the HMX molecule in its different polymorphs [97].

## 5.2. Pile-up avalanche model

The dislocation pile-up avalanche model for mechanically-induced hot spot generation is shown schematically in Figs. 15a-15d. The sequential pictures step through the following stages: (a) isothermal development of a pile-up under a shear stress, $\tau_1$, and blocked, for example, at a polycrystal grain boundary or at an internal crystal boundary or at crystal-to-crystal contacts produced in earlier deformation; (b) consequent achievement at larger dislocation number, $n_2$, and higher shear stress, $\tau_2$, of a critical stress concentration, $\tau_c$*, corresponding to collapse of the vobstacle; and, (c) dynamic release of the pile-up to form a localized hot spot [65]; see also the earlier presented model hot spot depictions shown in Fig. 7. Fig. 15d is included to indicate association of a discontinuous stress drop with the occurrence of significant hot spot generation, as had been discriminated among stress records compiled from calibrated drop-weight tests conducted on a number of energetic and related crystals [66]. The dislocation pile-up avalanche model in Fig. 15 builds onto an earlier continuum mechanics description for characterization of the release of a pile-up [101] and, also, builds onto a numerical model description that was given for dislocation pile-ups “breaking through” a polycrystal grain boundary region offering viscous resistance within a limited width of the boundary [102].

The temperature rise, $\Delta T$, for pile-up release was modeled from that reported earlier for the thermal dissipation of work associated with individual dislocation motions [103] but taken for the pile-up as a multiple Burgers vector dislocation of strength, *nb*, in the avalanche. With *n* being the number of

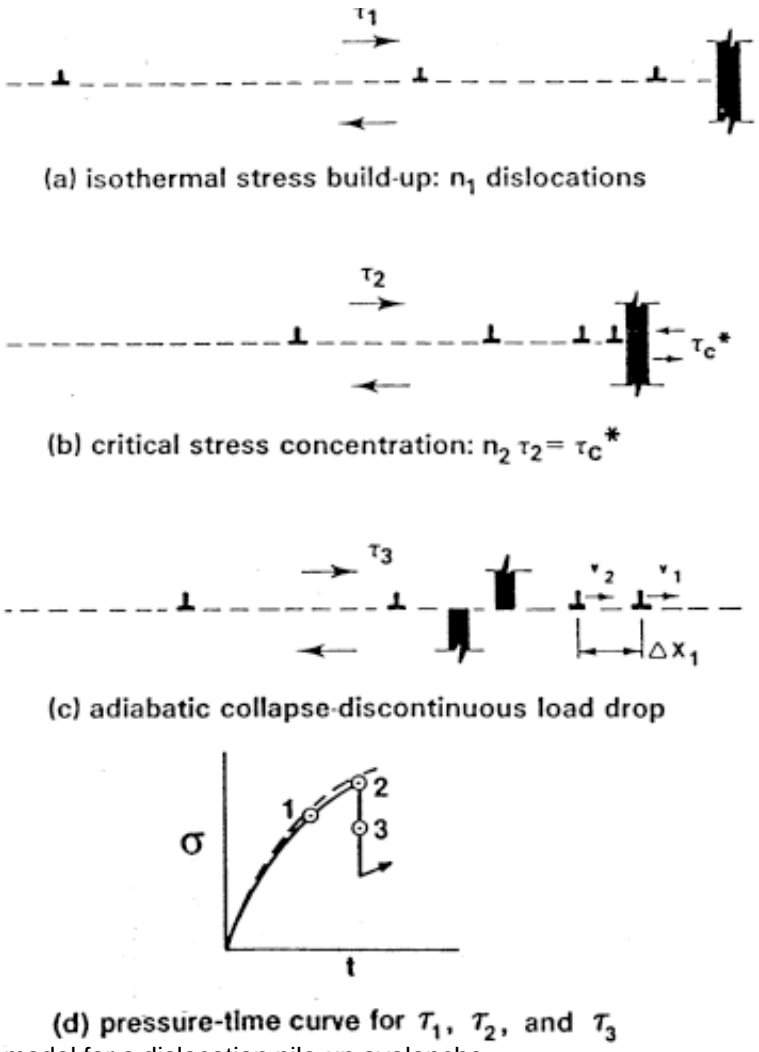


**Fig. 15.** Schematic model for a dislocation pile-up avalanche.

dislocations in the released pile-up, then in one approximation [65]

$$\Delta T = \left(k_s l^{1/2} / 16\pi\right)\left(2v / c^* bK\right)^{1/2}. \quad (4)$$

In Eq. (4), that applies for the combined material parameters ($2K/c^*vb$) < 1.0, $k_s$ is the microstructural shear stress intensity generated by the pile-up sufficient to cause pile-up breakthrough, $l$ is the grain or crystal diameter, $v$ is the dislocation velocity, $c^*$ is the specific heat at constant volume, and $K$ is the thermal conductivity. A largest $k_s$ occurs for shear induced cleavage cracking, as has been estimated for a number of materials [104]; and, the particular $k_s$ values listed in the fourth and fifth columns of Table 1 show that ($k_s/G$) is relatively large for RDX, PETN and AP. An immediate result worthy of notice in Eq. (4) is that a higher temperature rise is potentially generated for a larger crystal diameter.

Eq. (4) has been applied to explaining the crystal size dependence of the drop-weight impact results shown in Fig. 8 [63]. The influence of material loading rate was estimated from the dislocation velocity parameter, $v$, expressed as

$$v = v_0 \exp\left[-\left(G_0 - \int bA^* d\tau_{th}\right) / kT\right]. \quad (5)$$

In Eq. (5), $v_0$ is the reference dislocation velocity limited by the shear wave speed, $G_0$ is a reference Gibbs free energy, $A^*$ is the dislocation thermal activation area, and $k$ is Boltzmann's constant. This equation, that also forms the starting point for derivation of the so-called Z-A constitutive equations which have been applied to material dynamics calculations of structural face-centered cubic

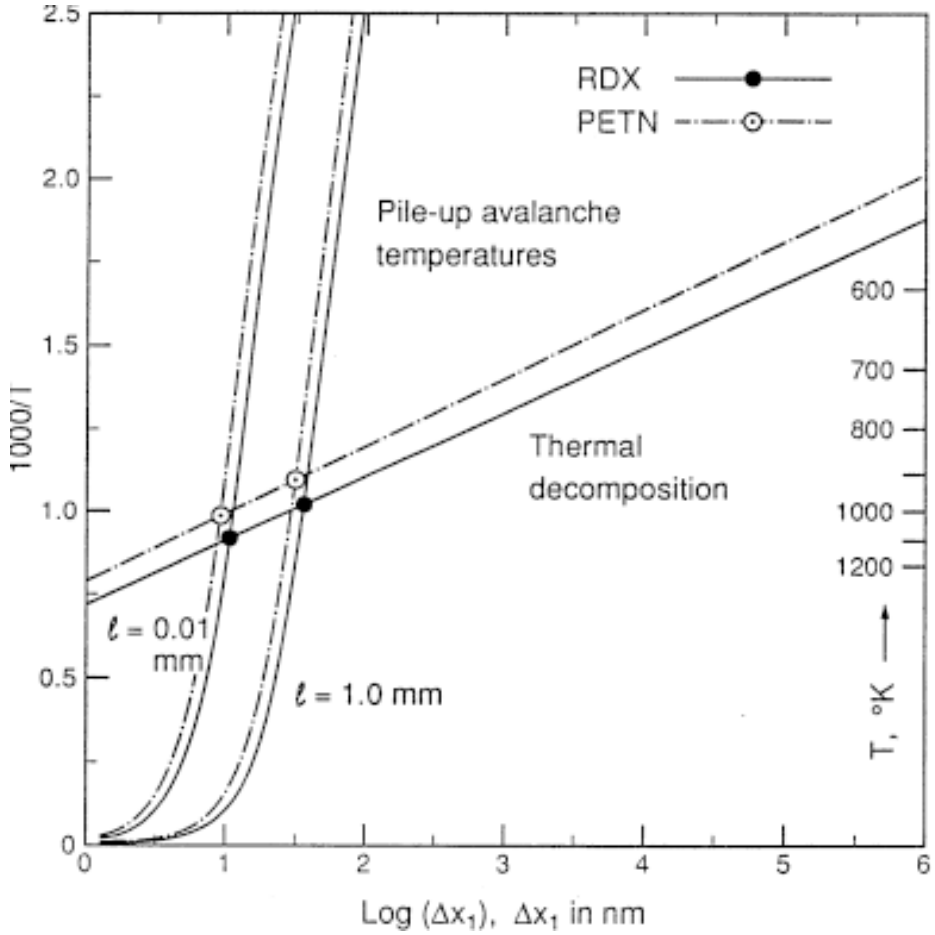


**Fig. 16.** Comparative dislocation pile-up avalanche and thermal decomposition temperatures for RDX and PETN crystals of different sizes; with the avalanche hot spot size determined by the dislocation separation at the pile-up tip just prior to release.

(fcc) and body-centered cubic (bcc) metal deformation behaviors [7], is seen to have a stress-modified Arrhenius form not unrelated to the thermal initiation equation analysis employed for the critical temperature dependence on hot spot size [9] and involved in the subsequently listed references [13-20]. With the several conditions: first, of the dislocation velocity being connected to the material shear strain rate in the normal thermally-activated manner and $A^*$ taken inversely proportional to $\tau_{th}$; and, secondly, the velocity taken to have a power exponent dependence on the material drop-weight sensitivity, then the result was obtained [68]

$$\log H_{50} \sim \log H_{50}^{*} + \left(kT / mW_0\right) \cdot \log\left(f\{\Delta T, T, \ldots\} l^{-1/2}\right). \quad (6)$$

In Eq. (6), $m$ is the power exponent for an assumed dependence of $\tau_{th}$ on $H_{50}$, $W_0$ is the constant product of $bA^*\tau_{th}$ and f{($\Delta T$, $T$, ...} represents a combination of the other factors in Eq. (4). Thus, for a fixed $\Delta T$ presumably being needed for a critical hot spot, Eq. (6) gives a reasonable explanation of the drop-weight height dependence on the inverse square root of the crystal size [21,69,104]. With the hot spot size taken proportional to the spacing of the leading dislocations at the pile-up tip prior to release, see Fig. 15, further comparison was made for RDX and PETN to show in Fig. 16 intersection of the mechanical and thermal model predictions for initiation of decomposition, as illustrated also for different crystal sizes. The crystal size effect is consistent with that shown in Fig. 8. In Fig. 16, RDX is seen to be relatively less sensitive to mechanical initiation because of the lesser thermal stability of PETN; an observation in general agreement with variously tabulated drop-weight measurements comparing material sensitivities.

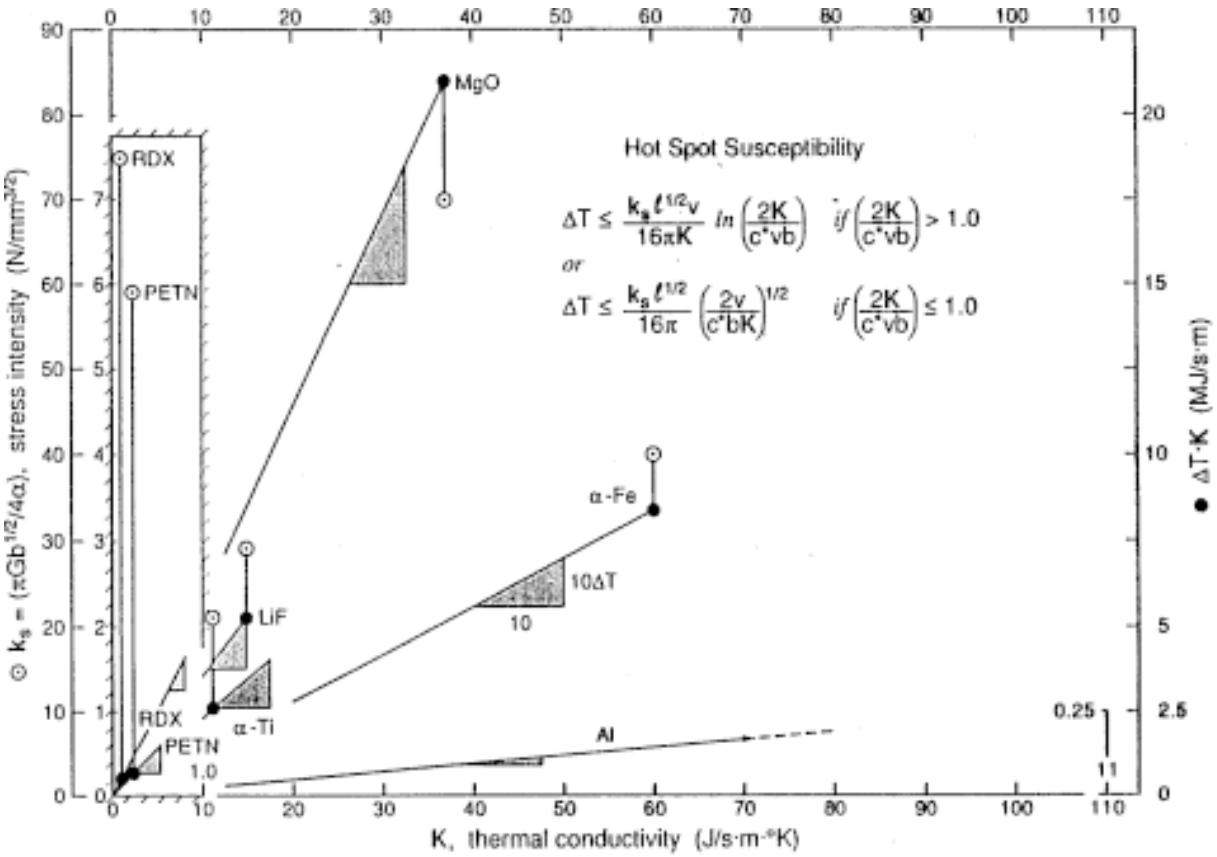


**Fig. 17.** The ratio of pile-up shear stress intensity for cracking, $k_s$, and thermal conductivity, $K$, as a criterion of susceptibility to hot spot development.

An important consideration relating to the pile-up avalanche model concerns the role of $k_s$ among other factors in the pile-up avalanche model description. For the combination of parameters ($2K/c^*vb$) ≥ 1.0, as is estimated to apply for metallic and ionic solids, Eq. (4) is replaced by

$$\Delta T = \left(k_s l^{1/2} v / 16\pi K\right) \ln\left(2K / c^* vb\right). \qquad (7)$$

On the basis of Eq. (7), the important material parameters controlling $\Delta T$ are $k_s$, $K$, and $v$. In order to make an estimation of energetic, ionic, and metallic material susceptibilities to hot spot generation at constant v, a plot of $k_s$ against $K$ was made as shown in Fig. 17. An increasing slope value drawn for any line to the variously plotted (open circle) points is indicative of an increasing susceptibility to hot spot initiation. To include the energetic $k_s$ and $K$ parameters along with the metallic and ionic ones in the figure, both the abscissa and ordinate scales were reduced by an order of magnitude, as shown by the inset rectangular graph including the data for RDX and PETN. Also, on the right hand ordinate scale of the larger figure frame, the product $K\Delta T$ is computed for the (filled circle) points plotted by assuming an upper-limiting shear wave speed for $v$. Thus, on both ($k_s/K$) and overestimated (principally because of $v$) $\Delta T$ bases, then, the energetic materials are shown among all of the materials to be relatively more susceptible to hot spot initiation. A very recent molecular dynamics (MD) model investigation of plasticity at a nanoindentation put into an RDX crystal has shown an appreciable temperature rise accompanying the process, also done at a relatively high loading rate [105]. Furthermore, the order of increasing slopes shown in Fig. 17 in the order of α-iron, α-titanium, and MgO as compared with a lowest slope for aluminum, are in line with increasingly greater shear banding susceptibilities being previously reported for these materials [106]. More recently, numerical computations have been reported [107] for the temperature rise associated with an avalanche break-

through of the viscous obstacle model given in [102].

Lastly here, relating to the furthest right-hand side column of Table 1, is the consideration of cleavage susceptibility, that can be taken as a measure of the generation of very localized plastic flow at a crack tip and, hence, be reflective of the localized generation of hot spots [81]. The parameter $(\gamma/Gb)^{1/2}$ whose numerical values are tabulated was obtained from a model estimation of the ratio of shear stresses needed either to propagate a crack by the Griffith mechanism or by a dislocation generation mechanism [107]. The listed numerical values for the ratio are consistent with the energetic materials being cleavage prone. They are certainly more so than is indicated by the higher values given for the ionic materials. The results are in line with the RDX *vs.* NaCl crystal comparison made on an IFM basis in Fig. 6. The dislocation generation part of the calculation was refined by more detailed evaluation of the dislocation nucleation mechanism but the improved criterion for brittleness appears to be approximately the same [109]. Even more recently, the subject has been reviewed with regard to better understanding the ductile-to-brittle transition in behavior that may occur on an individual dislocation basis, for example, when a material is subjected to dynamic loading [110]. And, there is the added issue of cleavage initiation being accomplished via dislocation pile-ups, as given emphasis here both for energetic materials and for their structural material counterparts too. A principal consideration in that regard is the dislocation pile-up explanation for the inverse square root of grain size dependence of the strength properties of structural materials [7] now having been shown to carry over to providing a better understanding of energetic crystal initiation behaviors, particularly, involving crystal size effects both in particle initiation behaviors and in combustion behavior associated with granular compaction.

## 5.3 Shock-induced initiations

Porosity, cracking, and plasticity influences are often intertwined in modeling the shock induced chemical decomposition properties of energetic crystal and composite materials [111]. MD simulations have proved to be an especially important tool in modeling of the shock-induced material behaviors for both energetic [112,113] as well as structural material [7,114,115] performances. A role for porosity in energetic material characterizations, which was carried over initially from the demonstrated sensitizing influence of gas bubbles in liquid explosives, as recently reviewed [116], has been and continues to be researched by the MD method applied at ever larger dimensions beginning from the nanoscale level for an isolated pore. From a solid mechanics viewpoint at the limiting larger continuum scale, the applied stress is known to be magnified locally by a factor of three times for a spherical void but this factor is magnified many times over in proportion to the aspect ratio of length to thickness in transforming the void into a crack of negligible thickness [117]. At such atomic level thickness, the crack is modeled equivalently on a continuum mechanics basis as a dislocation pile-up [118] consistent with the inverse square root of crack size dependence of strength properties described in the present report.

The preceding issue of dimensional scale at which porosity, cracking, and plasticity influences are to be accounted for may be traced by beginning from the smallest scale modeling involved in the ever increasing pursuit of more reliable MD computations. Early results for atomic- or molecular-scale pore collapses were obtained in relation to energetic material properties by modeling the stress-induced collapse of simple lattice point structures; see for example references [119,120]. In [113], beginning from an earlier hot spot associated Arrhenius-type description [13] and relating to pioneering orientation dependent PETN shock initiation measurements [121], not unrelated to that same consideration described for Fig. 5, reactive direction-dependent collisions among PETN or RDX molecules were investigated in relation to their respective crystal structures.

A latest investigation of porosity influence at the larger micron dimensional scale involves a crystal mechanics model of dynamic sub-surface pore collapse in an HMX crystal [122]. A constitutive equation incorporating dislocation drag was employed for tracking the role of dislocations during dynamic pore collapse; and, the crystal mechanics model was calibrated using a combination of MD and single crystal experimental results. Cracking and/or plastic shear under associated melting and non-melting conditions were investigated. Plasticity-associated jetting of material was demonstrated at the collapsing pore, without melting, but with occurrence of a relatively high dislocation density of $\sim 8 \cdot 10^9$ cm$^{-2}$, which is proposed to be typical for shock loading; however, see the above Eq. (3) and Table 1 consequences. The results suggest that pore collapse details depend on the interplay among pore size, wave structure as supported by

the initial dislocation density and dislocation kinetics, and other factors. Another forward-looking investigation [123], also referenced as an example of bridging length scales, has described a dislocation mechanics role involving shear on the [100](021) lattice-modeled system, as in Fig. 5, and as incorporated within a hydrocode model description of bullet penetration into a high explosive matrix. The study is remindful of the historical reference [8] and such modern practical assessments such as made in reference [72].

Dislocation density generations as compared with dislocation velocity-associated phonon drag influences are also of current research concern for structural materials with respect to shock-induced deformations and the relatively more recent method of testing at equivalent or higher imposed stress levels in a shock-less isentropic compression experiment (ICE). At relatively high shock pressures, the shear strains at all points within the nanometrically-scaled width of the shock front are not able to be relaxed by the remote displacements of an initially resident dislocation density behind the shock front nor by shear stress action applicable to the relatively few dislocation line intersections with the front [7,86,124]. Consequently, a nanoscale dislocation density is generated within a high pressure shock front and controls the shock-induced plastic strain rate. For the very differently imposed shock-less ICE-type loading, an opposite dislocation mechanism operates in that the uniformly increasing stress activates mobile dislocations from within the initially resident defect density but the relatively few dislocations, compared to the shock case, have to move at velocities approaching the shear wave speed and, hence, the constitutive deformation behavior is taken over by drag-control of the dislocation velocities [7,125]. The recent results reported for the comparison of high rate shock and ICE deformations of fcc copper and bcc iron materials [126] appear to be followed by analogous recent results reported for RDX crystals [127].

## 6. DISCUSSION

Explicitly indicated in Fig. 1 is the long (structural) “path” to be traveled in proceeding from the major descriptors for a composite material employed as a propellant (or explosive formulation) and the magnified view that is shown at expanded scale for an (010)[100] edge dislocation in its encompassing crystal lattice environment. Support for the considerable research effort that has been expended on energetic materials was applied with the purpose in mind of bridging the gap between the molecular and composite material properties [128]. And several of the listed article references given here have indicated that the composite material behavior could be tracked in a number of cases to the individual crystal properties. As indicated above, an extensive array of research diagnostics is being applied to achieving a better understanding of the shock-induced decomposition behavior for a full range of composite systems, especially, with regard to tracking the relevant hierarchical level at which critical events are controlled [111,129].

An additional case to illustrate the point of making a connection with the overall composite behavior is the search for an explanation of the onset of an unstable burn rate that may seemingly occur unpredictably during propellant combustion. The worry is for a deflagration-to-detonation (DDT) transition in behavior, which subject has been and continues to be a heavily researched topic [130]. A pioneering research description of internal stress effects associated with sub-surface cracking of crystals during combustion of HMX-based rocket propellant formulations was concerned with crystal size effects importantly suggested to be based in the $\beta$ - $\delta$ solid-state polymorphic transformation occurring at the higher pressures and temperatures in service [97]. Recently further connection has been proposed for the correlation of IFM cracking measurements made on HMX crystals and observed burning rate behaviors of HMX formulations [131].

The use of comparative inert material behaviors in composite formulations, for example, of sucrose extending from the individual crystal studies [36,58], and incorporated as a “PBS”, bonded with hydroxy-terminated-polybutadiene (HTPB) as for a PBX formulation, has been employed for the development of SHPB test procedures to be applied to energetic formulations, including observations of brittle fracture of the polymer binder at below glass transition temperatures [132,133]. Previous comment has been made in the present report concerning the importance of particle-to-particle contacts among the relatively hard energetic particles bonded within a softer polymer matrix [75,84]. In that regard, Fig. 18 is shown to indicate possible relevance of the material contiguity, *C*, parameter as a measure of such hard particle contacts and known to have significant influence on the mechanical behaviors of tool-cutting tungsten carbide-cobalt composite materials [118,134]. The figure is useful also to show relationship between the size and volume fraction dependencies of crys-

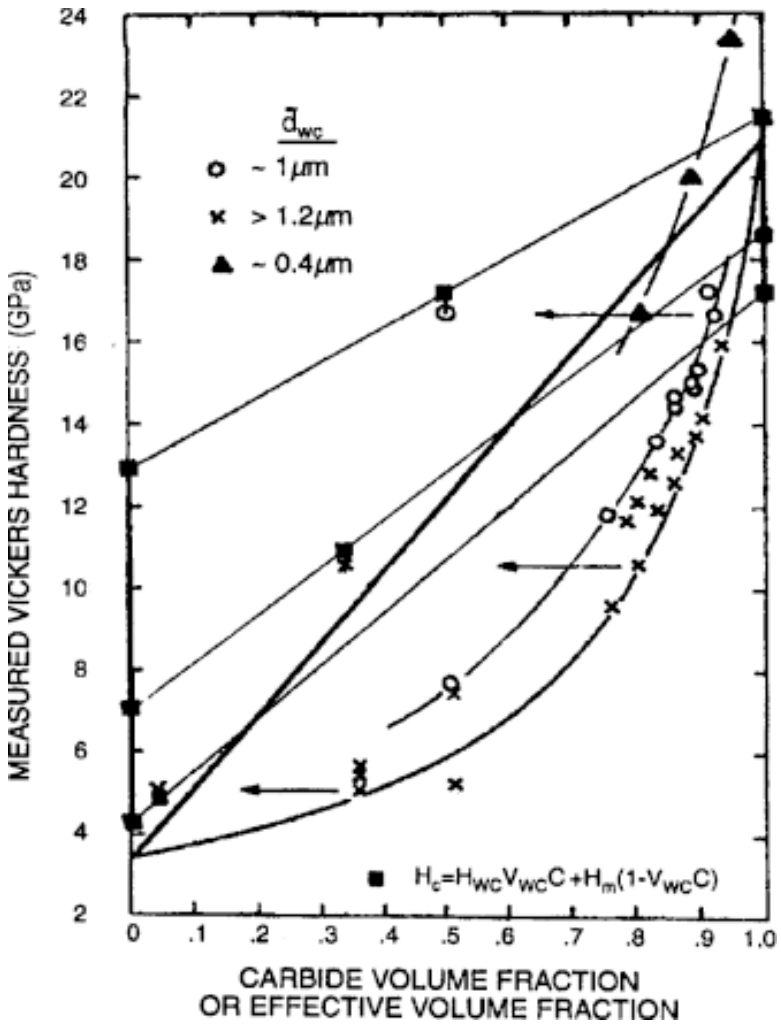


**Fig. 18.** The hardness as a function of volume fraction of tungsten carbide, $V_{WC}$, in WC-Co composite materials as dependent on the contiguity, $C$, measurement of particle-to-particle contacts and the sizes of carbide particles and the mean free path within the cobalt binder phase.

tal hardness for both particles and binder within a composite material.

In Fig. 18, the Vickers (diamond pyramid) hardness, $H$, is shown to depend on two volume fraction characteristics of the composite: the straightforward determination of $V_{WC}$, for the relative volume of tungsten carbide (WC) crystals; and, ($V_{WC}C$) for an effective volume fraction of particle-to-particle contacted material. The plotted cross, open circle, and filled triangle point measurements shown for the composite hardness measurements [135,136] are plotted on the abscissa $V_{WC}$ scale and show greater hardness values, beyond the $V_{WC}$ dependence, at smaller carbide particle sizes. Quantitative stereological investigation of the particle size effect led to the composite hardness expression

$$H = H_{wc}V_{wc}C + H_m\left(1-V_{wc}C\right), \tag{8}$$

in which $H_{WC}$ and $H_m$ are the separately determined hardness values of the individual carbide and cobalt matrix phases, respectively. A linear hardness dependence on the inverse square root of the particle size or grain size was determined separately for the tungsten carbide and cobalt constituents. Also, the size dependent hardness values determined for the two cross and one open circle measurement values marked in the figure by the horizontal arrows pointing leftwards were shifted to the

effective volume fraction points, $V_{WC}C$, as indicated for Eq. (8). As a first step for illustration of Eq. (8) application, the individual size-dependent hardness measurements applicable for both constituents of the three composite formulations were plotted as the filled square points shown on the terminal ordinate axes of the constituents. Then the linear dependence of the composite hardness on the effective volume fraction, $V_{WC}C$, was demonstrated for Eq. (8) by plotting the intermediate filled square points computed for the shifted measurement positions. Additional results on the cracking properties of this particular composite system have been reported also on a fracture mechanics basis [137]. It should be interesting to investigate whether similar behavior would be obtained for an appropriate energetic composite material especially as the contiguity factor, $C$, is indicated as well from the references, for example [75,84,85], made to the importance of particle-to-particle contacts being intimately involved in determining the composite material hot spot behaviors.

## 7. SUMMARY

A description has been given of experimental and model dislocation mechanics aspects of solid energetic crystal and composite material strength and chemical decomposition behaviors and also involving, as well, consideration in a number of instances of reference inert material properties. Dislocations are present at the beginning origination of any energetic crystal or composite formulation; and, the nature of the dislocations and their behaviors are shown here to be tied to the molecular bonding of the relatively complex energetic crystal lattices. On combined dislocation and crystal lattice bases, energetic crystals are shown to be elastically compliant, plastically strong, and especially susceptible to dislocation-assisted cleavage cracking. Indentation hardness, drop-weight impact, and stress wave loading techniques, in the latter case beginning with SHPB testing and extending to shock wave and ICE results, are shown collectively to provide important information about the strength and energy release properties of the materials, especially, as interpreted through the initiation and growth mechanisms described for localized hot spot developments. Emphasis is placed throughout the article on the crystal size dependencies observed for material strength properties and the sensitivities of the crystals to mechanically-induced decompositions. The total results point to advantages of greater strength and power dissipation being achieved for composite formulations fabricated from smaller particle-sized ingredients.

## ACKNOWLEDGMENTS

Professor Ilya Ovid'ko is thanked for inviting the present article. Appreciation is expressed to a number of colleagues: Herman Ammon and Zhu Yu Du, University of Maryland, for previous collaboration and providing the model crystal lattice pictures; to Wayne Elban, Loyola University Maryland, for collaboration on achievement of many of the results that are described in the present article; and also, to Frank Zerilli and now deceased Stephen Coffey, among other helpful scientists at the U.S. Naval Surface Warfare Center, Indian Head Division, for a number of collaborations too. Nathan Barton has provided helpful description of the results in Ref. 122. Valuable research periods with colleague associations were spent at the Cavendish Laboratory, University of Cambridge, U.K. and at the Energetic Materials Branch, Munitions Directorate, Eglin AFB, FL.

Note added in proof: A valuable description of laser ignition and initiation of explosives is given in N.K. Bourne // Proc. Roy. Soc. Lond. A 457 (2001) 1401.

## REFERENCES

[1] *Structure and Properties of Energetic Materials*, ed. by D.H. Liebenberg, R.W. Armstrong and J.J. Gilman (Materials Research Society, Pittsburgh, PA, 1993).

[2] *Decomposition, Combustion, and Detonation Chemistry of Energetic Materials*, ed. by T.B. Brill, T.P. Russell, W.C. Tao and R.B. Wardle (Materials Research Society, Pittsburgh, PA, 1996).

[3] *Synthesis, Characterization, and Properties of Energetic/Reactive Nanomaterials*, ed. by R.W. Armstrong, N.N. Thadhani, W.H. Wilson, J.J. Gilman and R.L. Simpson (Materials Research Society, Warrendale, PA, 2004).

[4] *Multifunctional Energetic Materials*, ed. by N.N. Thadhani, A.E. Gash, R.W. Armstrong and W.H. Wilson (Materials Research Society, Warrendale, PA, 2006).

[5]. R.W. Armstrong, In: *Advancements in Energetic Materials and Chemical Combustion*, ed. by K.K. Kuo and J. de Dios Rivera (Begell House, Inc.: N.Y., 2007), p. 331.

[6] R.W. Armstrong and J.F. Knott // *Mater. Sci. Tech*. **22** (2006) 379.
[7] R.W. Armstrong and S.M. Walley // *Intern. Mater. Rev*. **53** (2008) 105.
[8] B. Hopkinson // *Proc. Roy. Soc. Lond*. **213A** (1914) 437.
[9] T. Boddington, In: *Ninth Symposium (International) on Combustion* (Academic Press, N.Y., 1963), p. 287.
[10] E.M. Mas, B.E. Clements, A. Ionita and P. Peterson, In: *Shock Compression of Condensed Matter – 2005*, ed. by M.D. Furnish, M. Elert, T.P. Russell and C.T. White (Amer. Inst. Phys., Melville, N.Y., 2006) **CP845**, Part One, p. 487.
[11] J.C. Foster, D. Scott Stewart and K. Thomas, In: S*hock Compression of Condensed Matter – 2007*, ed. by M. Elert, M.D. Furnish, R. Chau, N.C. Holmes and J. Nguyen (Amer. Inst. Phys., Melville, N.Y., 2007) **CP955**, Part One, p. 369.
[12] D.E. Eakins and N.N. Thadhani, In: *Shock Compression of Condensed Matter – 2007*, ed. by M. Elert, M.D. Furnish, R. Chau, N.C. Holmes and J. Nguyen (Amer. Inst. Phys., N.Y., 2007) **CP955**, Part Two, p. 1025.
[13] H. Eyring // *Science* **199** (1978) 740.
[14] H. Eyring, M.S. Jhon and T. Ree, In: *Fast Reactions in Energetic Systems* (D. Riedel Publishing Co., Dordrecht, TN, 1981), p. 47.
[15] B.L. Wescott, D. Scott Stewart and W.C. Davis // *J. Appl. Phys.* **98** (2005) 053514.
[16] C.M. Tarver, In: *Shock Compression of Condensed Matter – 2005*, ed. by M.D. Furnish, M. Elert, T.P. Russell and C.T. White (Amer. Inst. Phys., Melville, N.Y., 2006) **CP845**, Part Two, p. 1026.
[17] P.M. Dickson, G.R. Parker, L.B. Smilowitz, J.M. Zucker and B.W. Asay, In: *Shock Compression of Condensed Matter – 2005*, ed. by M.D. Furnish, M. Elert, T.P. Russell and C.T. White (Amer. Inst. Phys., Melville, N.Y., 2006) **CP845**, Part Two, p. 1057.
[18] C.M. Tarver and S.K. Chidester, In: *Shock Compression of Condensed Matter – 2007,* ed. by M. Elert, M.D. Furnish, R. Chau, N.C. Holmes and J. Nguyen (Amer. Inst. Phys., Melville, N.Y., 2007) **CP 955**, Part One, p. 429.
[19] A.D. Wood, P.J. Haskins and M.D. Cook, In: *Intern. Conf. New Models and Hydrocodes for Shock Wave Processes in Condensed Matter*, ed. by R. Dormeval, V.Y. Klimenko, M. Zocher and F. Llorca (CEA Valduc, Dijon, FR, 2006), p. 64.
[20] V.G. Morozov, I.I. Karapenko, Yu.V. Yanilkin and O.N. Chernysheva, In: I*ntern. Conf. New Models and Hydrocodes for Shock Wave Processes in Condensed Matter*, ed. by R. Dormeval, V.Y. Klimenko, M. Zocher and F. Llorca (CEA Valduc, Dijon, FR, 2006), p. 153.
[21] R.W. Armstrong and W.L. Elban, In: *Dislocations in Solids*, ed. by F.R.N. Nabarro and J.P. Hirth (Elsevier, Amsterdam, TN, 2004), **12** p. 403.
[22] C.S. Choi and E. Prince // *Acta Cryst. A* **28** (1972) 2857.
[23] J.C. Gump, C.A. Stoltz and S.M. Peiris, In: *Shock Compression of Condensed Matter – 2007*, ed. by M. Elert, M.D. Furnish, R. Chau, N.C. Holmes and J. Nguyen (Amer. Inst. Phys., Melville, N.Y., 2007) **CP955**, Part One, p. 127.
[24] A.E.D.M. van der Heijden, C. Eldstater, W.P.C. De Klerk and A. Kjellstrom, In: *Advancements in Energetic Materials and Chemical Propulsion,* ed. by K.K. Kuo and J.de Dios Rivera (Begell House, Inc., N.Y., 2007), p. 342.
[25] J. Billingsley, In: *Shock Compression of Condensed Matter – 2007*, ed. by M. Elert, M.D. Furnish, R. Chau, N.C. Holmes and J. Nguyen (Amer. Inst. Phys., Melville, N.Y., 2007) **CP955**, Part Two, p. 891.
[26] R. Gilardi, In: *Structure and Properties of Energetic Materials*, ed. by D.H. Liebenberg, R.W. Armstrong and J.J. Gilman (Mater. Res. Soc., Pittsburgh, PA, 1993) **296**, p. 233.
[27] G.R. Miller and A.N. Garroway, *A Review of the Crystal Structures of Common Explosives, Part 1: RDX, HMX, TNT, PETN, and Tetryl* (Naval Research Laboratory, Washington, D.C., 2001) NRL/MR/6120-01-8585.
[28] P. Politzer and S. Boyd // *Struct. Chem.* **13** (2002) 105.
[29] C.J. Eckhardt and A. Gavezzotti // *J. Phys. Chem. B* **111** (2007) 3430.
[30] D.D. Dlott, S.A. Hambir and H. Yu, In: *Advancements in Energetic Materials and Chemical Propulsion*, ed. by K.K. Kuo and J. de Dios Rivera (Begell House, Inc., N.Y., 2007), p. 22.

[31] A. Rai, K. Park, D.G. Lee and M.R. Zachariah, In: *Advancements in Energetic Materials and Chemical Propulsion*, ed. by K.K. Kuo and J. de Dios Rivera (Begell House, Inc., N.Y., 2007), p. 87.
[32] R.L. McKenney, Jr. and T.R. Krawietz // *J. Energ. Mater.* **21** (2003) 141.
[33] W. Connick and F.G.J. May // *J. Cryst. Growth* **5** (1969) 65.
[34] A.E.D.M. van der Heijden and R.H.B. Bouma // *Cryst. Growth and Design* **4** (2004) 999.
[35] K.L. Kline, R.W. Armstrong, M.P. Kramer and D.W. Richards, In: *Shock Compression of Condensed Matter – 2003*, ed. by M.D. Furnish, Y.M. Gupta and J.W. Forbes (Amer. Inst. Phys., Melville, N.Y., 2004) **CP706**, Part Two, p. 779.
[36] W.L. Elban, D.B. Sheen and J.N. Sherwood // *J. Cryst. Growth* **137** (1994) 304.
[37] V. Stepanov, I.B. Elkina, T. Matsunaga, A.V. Chernyshev, E.N. Chesnokov, X. Zhang, N.L. Lavrik and L.N. Krasnoperov, In: *Advancements in Energetic Materials and Chemical Propulsion*, ed. by K.K. Kuo and J. de Dios Rivera (Begell House, Inc., N.Y., 2007), p. 74.
[38] A.E.D.M. van der Heijden, C.P.M. Roelands, Y.L.M. Creyton and R.H.B. Bouma, In: *Insensitive Energetic Materials; Particles, Crystals, Composites*, ed. by U. Teipel and M. Herrmann (Fraunhofer IRB Verlag, Stuttgart, DE, 2007), p. 41.
[39] I. Mikonsari, U. Teipel and H. Krober, In: *Insensitive Energetic Materials; Particle, Crystals, Composites* (Fraunhofer IRB Verlag, Stuttgart, 2007), p. 236.
[40] M. Herrmann and H. Fietzek // *Powder Diff.* **20** (2005) 105.
[41] M. Herrmann, I. Mikonsaari, H. Krause, M. Kaiser, R. Huhn, H. Sohn, M.H. Lefebvre, M. Alouaamari, C. Martin, A.E.D.M. van der Heijden, R.H.B. Bouma, J. Paap, J. Campos, I. Plaksin, R. Mendes, J. Rebeiro, J. Gois and S. Almada, In: *Insensitive Energetic Materials; Particles, Crystals, Composites* (Fraunhofer IRB Verlag, Stuttgart, DE, 2007), p. 260.
[42] T.M. Willey, T. van Buuren, J.R.I. Lee, G.E. Overturf, J.H. Kinney, J. Handly, B.L. Weeks and J. Ilavsky // *Propell. Explos. Pyrotech*. **31** (2006) 466.
[43] H. Klapper, In: *Characterization of Crystal Growth Defects by X-ray Methods*, ed. by B.K. Tanner and D.K. Bowen (Plenum Press, N.Y., 1980), p. 133.
[44] A.C. van der Steen and W. Duvalois, In: *ONR/TNO Workshop on Desensitization of Explosives and Propellants* (TNO Prins Maurits Laboratory, Rijswijk, TN, 1991) **3**, p. 1.
[45] I.T. McDermott and P.P. Phakey // *J. Appl. Cryst*. **4** (1971) 479.
[46] I.T. McDermott and P.P. Phakey // *Phys. Stat. Sol. (a)* **8** (1971) 505.
[47] W.L Elban, R.W. Armstrong, K.C. Yoo, R.G. Rosemeier and R.Y. Yee // *J. Mater. Sci.* **24** (1989) 1273.
[48] P.J. Halfpenny, K.J. Roberts and J.N. Sherwood // *J. Mater. Sci.* **19** (1984) 1629.
[49] P.J. Halfpenny, K.J. Robert and J.N. Sherwood // *Philos. Mag*. **53** (1986) 531.
[50] J.E. Field, S.M. Walley, W.G. Proud, J.E. Balzer, M.J. Gifford, S.G. Grantham, M.W. Greenaway and C.R. Siviour, In: *Synthesis, Characterization and Properties of Energetic/Reactive Nanomaterials*, ed. by R.W. Armstrong, N.N. Thadhani, W.H. Wilson, J.J. Gilman and R.L. Simpson (Mater. Res. Soc., Warrendale, PA, 2004), **800** p. 179.
[51] S.F. Son, T.J. Foley, V.E. Saunders, A.M. Novak, D.G. Tasker and B.W. Asay, In: *Multifunctional Energetic Materials*, ed. by N.N. Thadhani, R.W. Armstrong, A.E. Gash and W.H. Wilson (Mater. Res. Soc., Warrendale, PA, 2006), **896** p. 87.
[52] W.L. Elban and R.W. Armstrong, In: *Seventh Symposium (International) on Detonation* (Naval Surface Weapons Center, Silver Spring, MD, 1982) NSWC MP 82-334, p. 771.
[53] W.L Elban, J.C. Hoffsommer and R.W. Armstrong // *J. Mater. Sci.* **19** (1984) 552.
[54] H.G. Gallagher, P.J. Halfpenny, J.C. Miller, J.N. Sherwood and D. Tabor // *Philos. Trans. Roy. Soc. Lond. A* **339** (1992) 293.
[55] J.C. Hoffsommer, D.J. Glover and W.L. Elban // *J. Energ. Mater.* **3** (1985) 149.
[56] R. Behrens Jr. and S. Bulusu // *J. Phys. Chem.* **96** (1992) 8877.
[57] R.W. Armstrong and W.L. Elban // *Mater. Sci. Tech.* **22** (2006) 381.
[58] K.J. Ramos and D.F. Bahr // *J. Mater. Res.* **22** (2007) 2037.
[59] B.R. Lawn // *J. Appl. Phys.* **39** (1968) 4828.

[60] R.W. Armstrong and C.Cm. Wu // *J. Amer. Ceram. Soc.* **61** (1978) 102.
[61] R.W. Armstrong and W.L. Elban // *Mater. Sci. Eng. A* **111** (1989) 35.
[62] W.L. Elban // *J. Mater. Sci.* **14** (1979) 1008.
[63] R.W. Armstrong, W.L. Elban, A.L. Ramaswamy and C. Cm. Wu, In: *Challenges in Propellants and Combustion; 100 Years after Nobel*, ed. by K.K. Kuo (Begell House, Inc., N.Y., 1997), p. 313.
[64] D.A. Lucca, M.J. Klopfstein, O.R. Mejia, L. Rossettini and L.T. DeLuca // *Mater. Sci. Tech.* **22** (2006) 396.
[65] R.W. Armstrong, C.S. Coffey and W.L. Elban // *Acta Metall.* **30** (1982) 2111.
[66] S.N. Heavens and J.E. Field // *Proc. Roy. Soc. Lond. A* **338** (1974) 77.
[67] J. Namkung and C.S. Coffey, In: *Shock Compression of Condensed Matter – 2001*, ed. by M.D. Furnish, N.N. Thadhani and Y. Horie (Amer. Inst. Phys., Melville, N.Y., 2002) **CP620**, p. 1003.
[68] R.W. Armstrong, C.S. Coffey, V.F. DeVost, and W.L. Elban // *J. Appl. Phys.* **68** (1990) 979.
[69] R.W. Armstrong and W.L. Elban, In: *ONR/ LANL Workshop on the Fundamental Physics and Chemistry of Combustion, Initiation, and Detonation of Energetic Materials* (Chem. Propuls. Inform. Agency, The Johns Hopkins Univ, Baltimore, MD, 1992) CPIA Publ. 589, p. 367.
[70] R.G. Ames, In: *Multifunctional Energetic Materia*ls, ed. by N.N. Thadhani, R.W. Armstrong, A.E. Gash and W.H. Wilson (Mater. Res. Soc., Warrendale, PA, 2006), **896** p. 123.
[71] V.S. Joshi, In: *Shock Compression of Condensed Matter – 2007*, ed. by M. Elert, M.D. Furnish, R. Chau, N.C. Holmes and J. Nguyen (Amer. Inst. Phys., Melville, N.Y., 2007) **CP955**, Part Two, p. 945.
[72] J. Niles, S. Nicolich, D. Doll and N. Rassmussen, In: *Advancements in Energetic Materials and Chemical Propulsion*, ed. by K.K. Kuo and J. de Dios Rivera (Begell House, Inc., N.Y., 2007), p. 320.
[73] W.G. Proud, M.W. Greenaway, C.R. Siviour, H. Czerski, J.E. Field, D. Porter, P. Gould, P.D. Church and I.G. Cullis, In: *Multifunctional Energetic Materials*, ed. by N.N. Thadhani, R.W. Armstrong, A.E. Gash and W.H. Wilson (Mater. Res. Soc., Warrendale, PA, 2006), **896** p. 225.
[74] H. Moulard, In: *Ninth Symposium (International) on Detonation* (Office of the Chief of Naval Research, Arlington, VA, 1989) **1**, p. 18.
[75] X. Lu, Y. Hamate and Y. Horie, In: S*hock Compression of Condensed Matter – 2007*, ed. by M. Elert, M.D. Furnish, R. Chau, N.C. Holmes and J. Nguyen (Amer. Inst. Phys., Melville, N.Y., 2007) **CP955**, Part One, p. 397.
[76] W. Mock Jr. and J.T. Drotar, In: *Shock compression of Condensed Matter – 2007*, ed. by M. Elert, M.D. Furnish, R. Chau, N.C. Holmes and J. Nguyen (Amer. Inst. Phys. N.Y., 2007) **CP955**, Part Two, p. 971.
[77] A.L. Ramaswamy, H. Shin, R.W. Armstrong and C.H. Lee // *J. Mater. Sci.* **31** (1996) 6035.
[78] H.W. Sandusky, B.C. Glancy, D.W. Carlson, W.L. Elban and R.W. Armstrong // *J. Propuls. Power* **7** (1991) 518.
[79] B.C. Beard, H.W. Sandusky, B.C. Glancy and W.L. Elban // *J. Mater. Res.* **7** (1992) 3266.
[80] W.L Elban, H.W. Sandusky, B.C. Beard, and B.C. Glancy // *J. Propuls. Power* **11** (1995) 24.
[81] J.K. Dienes, Q.H. Zuo and J.D. Kershner // *J. Mech. Phys. Sol.* **54** (2006) 1237.
[82] M.J. Donache, Jr. and M.F. Burr // *J. Met*. **15** (1963) 849.
[83] R.C. Rowe and R.J. Roberts, In: *Pharmaceutical Powder Compaction Technology*, ed. by G. Alderborn and C. Nystrom (Marcel Dekker, Inc. N.Y., 1996), p. 283.
[84] S.J. Jacobs, H.W. Sandusky and W.L. Elban // *Powder Tech.* **89** (1996) 209.
[85] K.A. Gonthier // J. Appl. Phys. **95** (2004) 3482
[86] R.W. Armstrong (Trad.: J. Boileau) // *Rev. Scient. Tech. Defense* **16** (1992) 161.
[87] F.C. Frank // *Acta Cryst*. **4** (1951) 497.
[88] J.P. Hirth // *Acta Mater.* **57** (1999) 1.
[89] J. M. Thomas // *Endeavour* **29** (1970) 149.
[90] K.A. Gross // *J. Crystal Growth* **6** (1970) 210.
[91] Th. Scheffen-Lauenroth, H. Klapper and R.A. Becker // *J. Crystal Growth* **55** (1981) 557.
[92] M. Dudley, W. Si, S. Wang, C. Carter Jr., R. Glass and V. Tsvetkov // *Il Nuovo Cimento* **19D** (1997) 153.

[93] P. Pirouz // *Philos. Mag.* **78** (1998) 727.
[94] N. Ide, I. Okada and K. Kojima // *J. Phys.: Condensed Matter* **2** (1990) 5489.
[95] P.M. Robinson and H.J. Scott // *Acta Metall.* **15** (1967) 1581.
[96] Z.A. Dreger and Y.M. Gupta, In: *Shock Compression of Condensed Matter – 2007*, ed. by M. Elert, M.D. Furnish, R. Chau, N.C. Holmes and J. Nguyen (Amer. Inst. Phys., Melville, N.Y. , 2007) **CP955**, Part Two, p. 1239.
[97] R.J. Karpowitz and T.B. Brill // *AIAA J*. **20** (1982) 1586.
[98] R.W. Armstrong and F.J. Zerilli, In: *Advances in Twinning*, ed. by S. Ankem and C.S. Pande (The Metall. Soc. - AIME, Warrendale, PA, 1999), p. 67.
[99] H.H. Cady, In: *Structure and Properties of Energetic Materials*, edited by D.H. Liebenberg, R.W. Armstrong and J.J. Gilman (Mater. Res. Soc., Pittsburgh, PA, 1993), **296** p. 243.
[100] R.W. Armstrong, H.L. Ammon, Z.Y. Du, W.L. Elban and X.J. Zhang, In: S*tructure and Properties of Energetic Materials*, ed. by H.D. Liebenberg, R.W. Armstrong and J.J. Gilman (Mater. Res. Soc., Pittsburgh, PA, 1993), **296** p. 227.
[101] A.K. Head // *Philos. Mag.* **27** (1973) 531.
[102] F.P. Gerstle and G.J. Dvorak // *Philos. Mag.* **29** (1974) 1337.
[103] J.D. Eshelby and P.L. Pratt // *Acta Metall.* **4** (1956) 560.
[104] R.W. Armstrong and W.L. Elban // *Mater. Sci. Eng. A* **122** (1989) L1.
[105] Y.-C. Chen, K. Nomura, R.K. Kalia, A. Nakano and P. Vashishta // *Appl. Phys. Letts.* **93** (2008) 171908.
[106] R.W. Armstrong and F.J. Zerilli // *Mech. Mater.* **17** (1994) 319.
[107] W.R. Grise, In: *Multifunctional Energetic Materials*, ed. by N.N. Thadhani, R.W. Armstrong, A.E. Gash and W.H. Wilson (Mater. Res. Soc., Warrendale, PA, 2006), p. 177.
[108] R.W. Armstrong // *Mater. Sci. Eng.* **1** (1966) 251.
[109] J.R. Rice // *J. Mech. Phys. Sol.* **44** (1992) 235.
[110] G. Xu, In: *Dislocations in Solids*, ed. by F.R.N. Nabarro and J.P. Hirth (Elsevier B.V., Amsterdam, TM, 2004), **12** p. 81.
[111] H.R. James, In: *Shock Compression of Condensed Matter – 2007*, ed. by M. Elert, M.D. Furnish, R. Chau, N.C. Holmes and J. Nguyen (Amer. Inst. Phys., Melville, N.Y., 2007) **CP955**, Part Two, p. 931.
[112] J.W. Mintmire, D.H. Robertson and C.T. White // *Phys. Rev.* B **49** (1994) 14859.
[113] A. Landerville, I.I. Oleynik, M.A. Kozhushner and C.T. White, In: *Shock Compression of Condensed Matter – 2007*, ed. by M.Elert, M.D. Furnsih, R. Chau, N.C. Holmes and J. Nguyen (Amer. Inst. Phys., Melville, N.Y., 2007) **CP955**, Part One, p. 447.
[114] R.A. Lebensohn, E.M. Bringa and A. Caro // *Acta Mater.* **55** (2007) 261.
[115] G.E. Norman, A.Yu. Kuksin, V.V. Stegailov and A.V. Yanilkin, In: *Shock Compression of Condensed Matter – 2007*, ed. by M. Elert, M.D. Furnish, R. Chau, N.C. Holmes and J. Nguyen (Amer. Inst. Phys., Melville, N.Y., 2007) **CP955**, Part One, p. 329.
[116] S.M. Walley, J.E. Field and M.W. Greenaway // *Mater. Sci. Tech.* **22** (2006) 402.
[117] G.E. Dieter, In: *Mechanical Metallurgy*, Third Edition (McGraw-Hill, Inc., N.Y., 1986), p. 61.
[118] R.W. Armstrong // *Mater. Sci. Eng. A* **409** (2005) 24.
[119] F.A. Bandak, D.H. Tsai, R.W. Armstrong and A.C. Douglas // *Phys. Rev. B* **47** (1993) 11681.
[120] D.H. Tsai and R.W. Armstrong // *Chem. Phys. Reports* **14** (1995) 350.
[121] J.J. Dick // *J. Appl. Phys.* **81** (1997) 601.
[122] N.R. Barton, N.W. Winter and J.E. Reaugh // *Model. Simul. Mater. Sci. Eng*., in press.
[123] V.Y. Klimenko and I.Y. Kozyreva, In: I*ntern. Conf. New Models and Hydrocodes for Shock Wave Processes in Condensed Matter*, ed. by R. Dormeval, V.Y. Klimenko, M. Zocher and F. Llorca (CEA Valduc, Dijon, FR, 2006), p. 48.
[124] R.W. Armstrong, W. Arnold and F.J. Zerilli // *Metall. Mater. Trans. A* **38A** (2007) 2605.
[125] F.J. Zerilli and R.W. Armstrong // *Acta Mater.* **40** (1992) 1803.
[126] R.W. Armstrong, W. Arnold and F.J. Zerilli, In: *Shock Compression of Condensed Matter – 2007*, ed. by M. Elert, M.D. Furnish, R. Chau, N.C. Holmes and

J. Nguyen (Amer. Inst. Phys., Melville, N.Y., 2007) **CP955**, Part One, p. 623.
[127] M.R. Baer, M.L. Hobbs, C.A. Hall, D.E. Hooks, R.L. Gustavsen, D. Dattelbaum and S.A. Sheffield, In: *Shock Compression of Condensed Matter – 2007*, ed. by M. Elert, M.D. Furnish, R. Chau, N.C. Holmes and J. Nguyen (Amer. Inst. Phys., Melville, N.Y., 2007) **CP 955**, Part Two, p. 1165.
[128] R.W. Armstrong, H.L Ammon, W.L. Elban and D.H. Tsai // *Thermochim. Acta* **384** (2003) 303.
[129] I. Plaksin, C.S. Coffey, J. Campos, R. Mendes, J. Rebeiro and J. Gois, In: *Shock Compression of Condensed Matter – 2007*, ed. by M. Elert, M.D. Furnish, R. Chau, N.C. Holmes and J. Nguyen (Amer. Inst. Phys., Melville, N.Y., 2007) CP955, Part Two, p. 1427.
[130] R.R. Bernecker // *AAIA J.* **24** (1986) 82
[131] R.W. Armstrong, C.F. Clark and W.L. Elban, In: *Combustion of Energetic Materials*, ed. by K.K. Kuo and L. DeLuca (Begell House, Inc., NY, 2002), p. 354.
[132] D.R. Drodge, J.W. Addiss, D.M. Williamson and W.G. Proud, In: *Shock Compression of Condensed Matter – 2007*, ed. by M. Elert, M.D. Furnish, R. Chau, N.C. Holmes and J. Nguyen (Amer. Inst. Phys., Melville, N.Y., 2007) **CP955**, Part One, p. 513.
[133] C.R. Siviour, P.R. Laity, W.G. Proud, J.E. Field, D. Porter , P.D. Church, P. Gould and W. Huntington Thresher // *Proc. Roy. Soc. Lond. A* **464** (2008) 1229
[134] R.W. Armstrong, L. Ferranti Jr. and N.N. Thadhani // *Intern. J. Refract. Met. Hard. Mater.* **24** (2006) 11.
[135] H.C. Lee and J. Gurland // *Mater. Sci. Eng.* **33** (1978) 125.
[136] V. Richter and M. von Ruthendorf // *Intern. J. Refract. Met. Hard Mater.* **17** (1999) 141.
[137] R.W. Armstrong and O.Cazacu // *Intern. J. Refract. Met. Hard. Mater*. **24** (2006) 129.